Smart Structures and Systems, *Vol. 28, No. 2 (2021) 195-212*
DOI: https://doi.org/10.12989/sss.2021.28.2.195

Vibration analysis of sandwich beam with honeycomb core and piezoelectric facesheets affected by PD controller

Zeinab Soleimani-Javid [1], Saeed Amir*[1] and Zahra Khoddami Maraghi [2]

[1] *Department of Solid Mechanics, Faculty of Mechanical Engineering, University of Kashan, Kashan, Iran*
[2] *Mechanical Engineering Department, Engineering Faculty, Mahallat Institute of Higher Education, Mahallat, Iran*

(*Received February 9, 2020, Revised January 17, 2021, Accepted April 6, 2021*)

Abstract. Free vibration analysis of a sandwich beam with honeycomb core and piezoelectric face sheets, which is rested on the viscoelastic foundation is investigated. The thermal environment and the electric field are applied to this structure. Also, it is affected by the proportional-derivative (PD) controller. The amount of gain in this controller can affects the vibration frequency. The displacement components are expressed by improved high-order sandwich panel theory (IHSAPT) that considers continuity conditions for transverse shear stress at the interfaces and the zero transverse shear stresses conditions on the upper and lower surfaces of the beam and core flexibility. The motion equations are derived and solved by Hamilton's principle and Navier's method, respectively. This paper examines the effects of various parameters, such as the internal aspect ratio and the cell angle/thickness of the honeycomb core, temperature variations, viscoelastic environment, electric load, and control gain on its natural frequencies. The results show when the honeycomb core's to face sheet's thickness ratio increases, the beam dimensionless frequency increases, too. Also, by increasing the internal aspect ratio of honeycomb core, the frequency of sandwich beam decreases. The results of this study can be used to vibration control in aerospace engineering and constructions.

Keywords: free vibration; honeycomb core; improved high-order sandwich panel theory; piezoelectric facesheets; proportional-derivative controller; viscoelastic foundation

1. Introduction

Nowadays the use of sandwich composites and structures is approved by manufacturers due to weight loss and increased strength and safety. These structures are a great alternative to conventional metals used in the industry. Sandwich structures include three layers that consist of two layers of hard material with high elasticity modulus and, a light, soft core layer with very low elasticity modulus compared to the top and bottom layers. In many cases the core is most important part of the sandwich structures due to its mechanical properties therefore; in this article honeycomb core is applied. Honeycomb cores are widely used in the aerospace industry because of their weight and the ability to save on structure. It should be noted that honeycomb cores are produced in various forms, which hexagonal type has the most used. In 1915 Hugo Junkers who was German engineer explored the idea of a honeycomb core within a laminate structure and then patented the first honeycomb cores for aircraft applications. He described in detail the positive benefits of honeycomb structure rather than fabric-covered aircraft structures by metal sheets. In the early 1990s, Lorna and Gibson (1989) wrote a book entitled "cellular structure" on porous, foam material and honeycomb structure and examined the different properties of these materials under different conditions, then Fu and Yin (1999) improved these relations and expressed Gibson's modified equations. Torabi *et al*. (2019) examined vibration analysis of a sandwich plate which consisted of homogeneous isotropic face sheets and cantilever trapezoidal honeycomb core. The plate has been modeled based on aerodynamic pressure of external flow with the desired flow. Yongqiang and Dawei (2009) investigated vibration behavior of a symmetric honeycomb in a sandwich panels. This structure is assumed to be acted by water. They used the Gibson's relations to determine mechanical properties. Şakar and Bolat (2015) have studied vibration of honeycomb sandwich beam that was made by aluminum. They used the continuum and 3D model. Then they compared this research result with experimental finding. Zhang *et al*. (2017) analyzed the free vibrations of sandwich beams that the core is made of combination of honeycomb and corrugation. They used finite element method to predict their mode shape and natural frequencies. Cheng *et al*. (2016) examined the vibration of sandwich beam consisted of honeycomb core and homogenous thin facesheets. They used Ritz method to solve the governing equations.

Centuries ago, people used the effective of piezoelectric properties and later this effect was named piezoelectricity by a Scottish physicist. The first time effect of piezoelectric was introduced by Ren-Just Hay a French miner. Yue *et al*. (2016) have studied about a micro scale beam modeled by piezoelectricity. They also obtained free vibration and static bending from a simply supported piezoelectric nano beam.

*Corresponding author, Assistant Professor,
E-mail: samir@kashanu.ac.ir;
saeid_amir27111@yahoo.com

ISSN: 1738-1584 (Print), 1738-1991 (Online)

Amir *et al*. (2018) investigated the buckling of sandwich plate with piezoelectric facesheets and nanocomposite core. They assumed there was the flexoelectricity effect in each layer also they used the first order shear deformation theory to analyze the critical buckling due to its more accurate result. Ghorbanpour Arani *et al*. (2018) presented vibration response in a sandwich plate with nano composite facesheets, which included carbon nano tube and piezoelectric matrix and also magneto rheological fluid core. Magnetic and electric fields were applied to this structure then they examined the influence of these fields and geometrical parameters on nondimensional natural frequencies. Arefi and Zenkour (2017) have studied bending behavior a sandwich nano plate which integrated with piezoelectric facesheets and affected by temperature load and applied voltage. Arshid and Khorshidvand (2018) examined the free vibration behavior on a circular plate which the core and the facesheets consist of porous material and piezoelectric actuators, respectively. They have neglected of shear deformation due to the low thickness of the structure in classical plate theory.

One of the most important and accurate sandwich structures' theories that investigate the deformations and strains in each layer is higher-order sandwich panel theory (HSAPT). In this theory there are interlaminar stresses between a layer in structure with its top and bottom layers and actually must be stress continuity condition in it, but the mechanical properties are different in contiguous layers, thus the stiffness matrixes in these two layers are been different. Since the stresses are equal, but the stiffness matrixes are different, consequently the strains in two contiguous will not be equal.

This theory was introduced by Frostig *et al*. (1992) in 1990s for the first time, thus this was called Frosting theory. He also considered the flexibility of the core in this theory. The sandwich beam that he studied included a soft, thick core to its facesheets. In another work, Frostig and Thomsen (2004) presented this theory for free vibration of sandwich panels. They calculated governing equations of the structure in two different ways and derived analytically answer of equations for a simply supported sandwich plate. Malekzadeh *et al*. (2005) investigated the vibrations of sandwich panels with viscoelastic flexible core. They improved the Frosting theory and the most important difference is the displacement field for the facesheets. This theory was called improved higher order sandwich panels theory (IHSAPT) and has been used in various articles. For example, Moradi-dastjerdi and Malek-mohammadi (2016) have studied buckling behavior of a sandwich plates with nano composite facesheets and composite core by using the IHSAP theory and used the Navier's method to solve the equations. They considered third order theory in each layer. Biaxial wrinkling and bending analysis in a sandwich plate with soft core using IHSAP theory were investigated by Khalili *et al*. (2013) and Kheirikhah *et al*. (2012a), respectively. Also, Salami *et al*. (2016) used this theory for bending analysis of sandwich beams with moderately thick facesheets and they had considered the compatibility conditions at the interfaces, also they solved the equations by using the Navier's method.

Controllers are just like communication devices to the systems and a controller is like an industrial process mastermind. The control operation is as follows, the vibrational movements of the structure are sensed by piezoelectric sensors and then the corresponding control signal will be sent to the actuator to obtain a damped response. Yiqi and Yiming (2010) studied about active vibration control and nonlinear dynamic responses for a kind of plate with piezoelectric functionally graded (FG) material. They considered the negative velocity feedback control algorithm to perform nonlinear active vibration control in that structure. AkhavanAlavi *et al*. (2019) presented a micro Reddy beam with piezoelectric facesheets reinforced by carbon nano tubes and the facesheets are made by sensor and actuator. They used the LQR algorithm to control vibrations and find an appropriate feedback controller. In the other work vibrations analysis of sandwich microplates with sensor and actuator facesheets and nanocomposite core are investigated by Ghorbanpour Arani *et al*. (2016a). The structure was rested on orthotropic Pasternak foundation. They employed a partial- differential (PD) controller in order to control the frequency by closed-loop control sensors and actuators. Also, Phung-van *et al*. (2015) investigated analysis of composite plates which integrated piezoelectric sensor and actuator facesheets layer and a composite layer at the core. They applied a third-order shear deformation theory to show the displacement field. In addition, a velocity feedback control algorithm through a closed-loop control with bonded distributed piezoelectric sensors and actuators was used for the active control of this structure. The thermal vibrations analysis of functionally graded (FG) shell included magnetostrictive layer using the generalized differential quadrature (GDQ) method was presented by Hong (2013). The FGM shell was analyzed with and without negative velocity feedback under conditions of different magnetic field values. The results of this work have been shown by velocity feedback and choosing an appropriate controller. Nezami and Gholami (2015) studied the properties of active aerostatic vibration and vibration control of sandwich panels which has three types different honeycomb models. They used linear quadratic regulator (LQR) optimal control method for vibration control. This sandwich panel is composed of piezoelectric surfaces, with the actuator and sensor on the top and bottom layer, respectively.

The literature review by the authors showed that no researcher provided a study about sandwich beam with the following given specifications, so the authors motivated to conduct it. The current study is aimed to analyze vibrations of a three-layered sandwich beam with a honeycomb core made of aluminum and PZT4 piezoelectric face sheets and presented a higher-order beam theory. The piezoelectric face sheets are affected by the PD controller, which can be effective on the frequencies. The structure is also placed in a thermal and viscoelastic environment. The main novelties of the present research lay in the displacement continuity equations at the interfaces. This continuity theory is more close to the real conditions and provides an accurate answer to the equations. This type of honeycomb structure with the PD controller and by using this displacement theory had

been never investigated. The findings of this work will help to design and create more optimal engineering and smart structures such as sensors and actuators, as well as the honeycomb structures due to the light constructions, are applied in air vehicles.

This article has been investigated the free vibration analysis of a sandwich beam with honeycomb core and the piezoelectric layers. This beam is rested on elastic foundation, also the effect of thermal load on stresses of layers and effect of electric field on the sensor and actuator layers is assumed. This sandwich beam is affected by a simple control algorithm, PD controller and the amount of control gain could affect the vibration frequencies. This paper has been tried to use the newest theories includes IHSAPT, that considers the effect of all stress conditions and the flexibility of the core. This article has analyzed the free vibrations of this sandwich beam by means of Navier's solution method. The results of this study show the effect of different parameters such as cell angle, internal aspect ratio and value of cell thickness and geometrical parameters are considered and can be concluded by enhancing the core thickness, the beam natural frequency increased.

2. Mathematical formulation

The sandwich beam is composed of two piezoelectric layers at the top and bottom and a honeycomb core. h_t, h_b, and h_c are the thicknesses of the top, bottom facesheets and core, respectively, also the total thickness and the length of the beam are indicated by H and L, respectively. This structure is rested on the viscoelastic substrate as it is seen in Fig. 1.

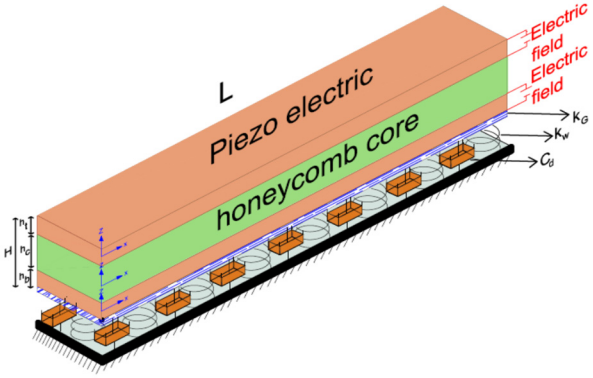

Fig. 1 Geometry of a sandwich beam resting on viscoelastic foundation

2.1 Kinematic relations

In this section, the displacement fields for core and facesheets are based on IHSAP theory. As mentioned the core's thickness is more than its facesheet. The displacement field in the thickness direction is higher order at the core so the displacement fields for the each of layers are obtained in Eqs. (1)-(2), respectively (Khalili *et al.* 2013).

$$\begin{aligned} u_c(x,z,t) &= u_{0c}(x,t) + zu_{1c}(x,t) \\ &\quad + z^2u_{2c}(x,t) + z^3u_{3c}(x,t) \\ w_c(x,z,t) &= w_{0c}(x,t) + zw_{1c}(x,t) + z^2w_{2c}(x,t) \end{aligned} \tag{1}$$

u_{0c} and w_{0c} are the in-plane and vertical displacement in x and z directions, respectively. (u_{1c}, u_{2c}, u_{3c}, w_{1c}, w_{2c}) are the unknown displacements that calculated by using the displacement continuity condition at the top and bottom interfaces.

$$\begin{aligned} u_i(x,z,t) &= u_{0i}(x,t) + zu_{1i}(x,t) \\ &\quad + z^2u_{2i}(x,t) + z^3u_{3i}(x,t) \\ w_i(x,z,t) &= w_{0i}(x,t) \end{aligned} \tag{2}$$

u_0 and w_0 (i = t, b) are the in-plane and vertical displacement in x and z direction, respectively and also other parameters (u_0, u_1, u_2) are unknown in-plane displacements (Khalili *et al.* 2013).

The facesheets and core linear strain relations can be defined as

$$\begin{aligned} \varepsilon_{xxc} &= \frac{\partial u_{0c}(x,t)}{\partial x} + z\left(\frac{\partial u_{1c}(x,t)}{\partial x}\right) + z^2\left(\frac{\partial u_{2c}(x,t)}{\partial x}\right) + z^3\left(\frac{\partial u_{3c}(x,t)}{\partial x}\right) \\ \varepsilon_{zzc} &= w_{1c}(x,t) + 2zw_{2c}(x,t) \\ \gamma_{xzc} &= \frac{\partial w_{0c}(x,z,t)}{\partial x} + z\left(\frac{\partial w_{1c}(x,z,t)}{\partial x}\right) + z^2\left(\frac{\partial w_{2c}(x,z,t)}{\partial x}\right) + u_{1c}(x,t) + 2zu_{2c}(x,t) \\ &\quad + 3z^2u_{1c}(x,t) \\ \varepsilon_{xx} &= \frac{\partial u_0(x,t)}{\partial x} + z\left(\frac{\partial u_1(x,t)}{\partial x}\right) + z^2\left(\frac{\partial u_2(x,t)}{\partial x}\right) + z^3\left(\frac{\partial u_3(x,t)}{\partial x}\right) \\ \varepsilon_{zz} &= 0 \\ \gamma_{xz} &= \frac{\partial w_0(x,z,t)}{\partial x} + u_1(x,t) + 2zu_2(x,t) + 3z^2u_1(x,t) \end{aligned} \tag{3}$$

2.2 Compatibility equations

In this theory, the core and facesheets are fully bonded. So, there are displacement continuity equations between the interfaces which can be obtained as follows (Dariushi and Sadighi 2015).

$$\begin{aligned} u_t\left(z_t = -\frac{h_t}{2}\right) &= u_c\left(z_c = \frac{h_c}{2}\right), \\ u_b\left(z_b = \frac{h_b}{2}\right) &= u_c\left(z_c = -\frac{h_c}{2}\right) \\ w_t\left(z_t = -\frac{h_t}{2}\right) &= w_c\left(z_c = \frac{h_c}{2}\right), \end{aligned} \tag{4}$$

$$w_b\left(z_b=\frac{h_b}{2}\right)=w_c\left(z_c=-\frac{h_c}{2}\right) \tag{4}$$

2.3 Continuity equations

As mentioned, the innovation of this theory is the investigation of the displacement continuity equations at the interfaces, in other words, the stress continuity at interfaces should be exist (Moradi Dastjerdi *et al*. 2016).

$$\begin{aligned} C_{55t}\gamma_{xzt}\left(x,z=\tfrac{h_t}{2}\right)&=C_{55c}\gamma_{xzc}\left(x,z=-\tfrac{h_c}{2}\right)\\ C_{55b}\gamma_{xzb}\left(x,z=-\frac{h_b}{2}\right)&=C_{55c}\gamma_{xzc}\left(x,z=\frac{h_c}{2}\right)\end{aligned} \tag{5}$$

And the transverse shear stresses are assumed to be zero at the external surface.

$$\begin{aligned} C_{55t}\gamma_{xzt}\left(x,z_t=\frac{h_t}{2}\right)&=0,\\ C_{55b}\gamma_{xzb}\left(x,z_b=-\frac{h_b}{2}\right)&=0\end{aligned} \tag{6}$$

According to the above equations can be concluded the transverse shear strains are equal to zero at external surfaces.

$$\gamma_{xzt}\left(x,z_t=\frac{h_t}{2}\right)=\gamma_{xzb}\left(x,z_b=-\frac{h_b}{2}\right)=0 \tag{7}$$

2.4 Stress-strain relations

2.4.1 Honeycomb core

The strain-stress relations are used to obtain stresses corresponding to strains. The strain stress relation of the honeycomb core is shown according to Hooke's law

$$\begin{bmatrix}\sigma_{xc}\\ \sigma_{zc}\\ \tau_{xzc}\end{bmatrix}=\begin{pmatrix}C_{11c} & C_{13c} & 0\\ C_{13c} & C_{33c} & 0\\ 0 & 0 & C_{55c}\end{pmatrix}\begin{Bmatrix}\varepsilon_{xxc}\\ \varepsilon_{zzc}\\ \gamma_{xzc}\end{Bmatrix} \tag{8}$$

And C_{ij} are stiffness matrices components that have been shown in composite references, thus it can be obtained as follows

$$C_{55c}=G_m,\quad C_{13c}=\nu_c C_{11c},\quad C_{11c}=C_{33c}=\frac{E_c}{1-{\nu_c}^2} \tag{9}$$

2.4.2 Piezoelectric facesheets

The strain-stress relations are also shown for the piezoelectric facesheets (Fallah and Ebrahimnejad 2014)

$$\begin{bmatrix}\sigma_x\\ \tau_{xz}\end{bmatrix}=\begin{pmatrix}C_{11} & 0\\ 0 & C_{55}\end{pmatrix}\begin{Bmatrix}\varepsilon_{xx}\\ \gamma_{xz}\end{Bmatrix}-\begin{pmatrix}0 & e_{31}\\ e_{15} & 0\end{pmatrix}\begin{Bmatrix}E_x\\ E_z\end{Bmatrix} \tag{10}$$

$$\begin{bmatrix}D_x\\ D_z\end{bmatrix}=\begin{pmatrix}0 & e_{15}\\ e_{31} & 0\end{pmatrix}\begin{Bmatrix}\varepsilon_{xx}\\ \gamma_{xz}\end{Bmatrix}-\begin{pmatrix}k_{11} & 0\\ 0 & k_{33}\end{pmatrix}\begin{Bmatrix}E_x\\ E_z\end{Bmatrix} \tag{11}$$

k_{11}, k_{33} and e_{31}, e_{15} are dielectric and piezoelectric coefficients, and D_i, E_i ($i = x, y, z$) are electric displacement and electric field, respectively, which the electric field is calculated in terms of electric potential ($\Phi = \Phi(x, z, t)$) (Arshid *et al*. 2020a)

$$E_x=-\frac{\partial\Phi}{\partial x}E_y=-\frac{\partial\Phi}{\partial y}E_z=-\frac{\partial\Phi}{\partial z} \tag{12}$$

The potential function $\Phi(x,z,t)$ shows to satisfy the electric boundary conditions (Ebrahimi and Daman 2017). Φ is distributions of the electric potential across the thickness direction, Maxwell's relations have been used to satisfying sensor and actuator layers, thus the following equation is written (Ghorbanpour Arani *et al*. 2016b)

$$\begin{aligned}\Phi^a(x,z,t)&=sin\left(\frac{\pi\left(z-\frac{h_c}{2}\right)}{h_a}\right)\Phi^a(x,t)\\ &\quad+\frac{(z-h_c/2)V_0}{h_a}\\ \Phi^s(x,z,t)&=sin\left(\frac{\pi\left(-z-\frac{h_c}{2}\right)}{h_s}\right)\Phi^s(x,t)\end{aligned} \tag{13}$$

in which superscripts a and s denote actuator and sensor faces. V_0 is applied voltage on actuator layer and the electric potential, $\Phi(x, t)$ is on the mid surface of the piezoelectric layers.

3. Equations of honeycomb core

It is indicated solitary honeycomb structures usually do not benefit and are used to at a sandwich structure in the middle of two other layers. To determine the properties of this structure, (Fu and Yin 1999) used the improved equations (Lorna and Gibson 1989) so the equations are

$$\begin{aligned}\rho_c&=\rho\frac{(2+\varphi_0)}{2\cos\theta_0\,(\varphi_0+\sin\theta_0)}\gamma_0\\ E_c&=E\frac{\cos\theta_0\,(1-\gamma_0^2\cot^2\theta_0)}{\sin^2\theta_0\,(\varphi_0+\sin\theta_0)}\gamma_0^3\\ \nu_c&=\frac{\cos^2\theta_0\,(1-\gamma_0^2\csc^2\theta_0)}{\sin\theta_0\,(\varphi_0+\sin\theta_0)}\\ G_c&=E\frac{(\varphi_0+\sin\theta_0)}{\varphi_0^2(1+2\varphi_0)\cos\theta_0}\gamma_0^3\end{aligned} \tag{14}$$

where $\varphi_0=\frac{h_0}{l}$, $\gamma_0=\frac{t}{l}$, and symbols θ_0, t, l are shown in Fig. 2.

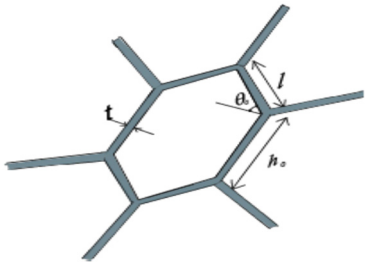

Fig. 2 Schematic of a honeycomb cell

ν_c, G_c, E_c, ρ_c are the Poisson's ratio, shear modulus, elastic modulus and density of the honeycomb core, respectively.

4. PD controller

A PD controller is used to control system behavior. Therefore, the electric potential of the actuator layer can be written as Eq. (15), which is the sum of the electric potential of the sensor layer and its derivative respect to time (Phung-van *et al*. 2015).

$$\Phi^a(x,z,t) = K_p\Phi^s(x,z,t) + K_d\frac{\partial}{\partial t}(\Phi^s(x,z,t)) \quad (15)$$

where K_P and K_d represent proportional and derivative control coefficients, respectively.

5. Energy method

Among the various methods for achieving equations of motion, the present research has used the energy approach for its comprehensiveness. In the energy method, the total potential energy includes strain energy, kinetic energy, and external loads (Zhang *et al*. 2019)

$$\Pi = U - (T + W) \quad (16)$$

5.1 Strain energy

In this study, the total potential energy of this system is equal to the sum of the strain energy of the beam model and the strain energy obtained from the continuity conditions in this structure (Nguyen *et al*. 2016, 2017).

$$U = U_s + U_L \quad (17)$$

$$U_s = \frac{1}{2}\int_0^L \int_{A_i} (\sigma_{xx}{}^i\varepsilon_{xx}{}^i + \sigma_{zz}{}^i\varepsilon_{zz}{}^i + \tau_{xz}{}^i\gamma_{xz}{}^i)dA_i dx \quad (18)$$

$$\begin{aligned} U_L = \int_0^L [&\lambda_x^t\left(u_t\left(z_t=\frac{h_t}{2}\right)-u_c\left(z_c=-\frac{h_c}{2}\right)\right)+\lambda_z^t\left(w_t\left(z_t=\frac{h_t}{2}\right)-w_c\left(z_c=-\frac{h_c}{2}\right)\right)\\ &+\lambda_x^b\left(u_b\left(z_b=-\frac{h_b}{2}\right)-u_c\left(z_c=\frac{h_c}{2}\right)\right)+\lambda_z^b\left(w_b\left(z_b=-\frac{h_b}{2}\right)-w_c\left(z_c=\frac{h_c}{2}\right)\right)\\ &+\lambda_{xz}^t\left(\gamma_{xz}{}^t\left(z_t=-\frac{h_t}{2}\right)\right)-\lambda_{xz}^b\left(\gamma_{xz}{}^b\left(z_b=\frac{h_b}{2}\right)\right)+\lambda_{xz}^{tc}(C_{55}{}^t\gamma_{xz}{}^t\left(z_t=\frac{h_t}{2}\right)-C_{55}{}^c\left(\gamma_{xz}{}^c\left(z_c=-\frac{h_c}{2}\right)\right)\\ &+\lambda_{xz}^{bc}(C_{55}{}^b\gamma_{xz}{}^b\left(z_b=-\frac{h_b}{2}\right)-C_{55}{}^c\left(\gamma_{xz}{}^c\left(z_c=\frac{h_c}{2}\right)\right)]dx \end{aligned} \quad (19)$$

where i (i = t, b, c) represents the top, bottom, and core layers.

λ is the Lagrangian coefficient that is added to the differential equations to solve them. λ_I (I = x, z), (j = t, b) represents four Lagrangian coefficients for the interlayer compatibility conditions at the top and bottom layers. $\lambda_{iz}{}^j$ (I = x), (j = t, b) also shows two Lagrangian coefficients for zero shear stress conditions at the top and bottom beam surface, $\lambda_{iz}{}^{jc}$ (I = x), (j = t, b) are two Lagrangian coefficients to indicate the continuity conditions at transverse shear stress between layers (Kheirikhah *et al*. 2012b, Nguyen *et al*. 2019).

5.2 Kinetic energy

In order to the displacement of the sandwich beam in directions x and z, the velocities are defined in these directions and the kinetic energy is written as follows, that $\rho_i(t,b,c)$ shows the density (Arshid *et al*. 2019)

$$T = \frac{1}{2}\rho_i\int_0^L\left[\int_A\left[\left(\frac{\partial U^i}{\partial t}\right)^2+\left(\frac{\partial W^i}{\partial t}\right)^2\right]dAdx \quad (20)$$

5.3 External work

5.3.1 Viscoelastic environment

The effect of viscoelastic environment for the lower layer of the sandwich beam is appeared in the external work, so it can be seen as following

$$W_1 = \int_A 1/2\left[F_{foundation}w_{0b}(x,t)\right]dA \quad (21)$$

$$\begin{aligned} F_{foundation} = K_W w_{0b}(x,t) - K_G\frac{\partial^2}{\partial x^2}w_{0b}(x,t)\\ +C_d\frac{\partial}{\partial t}w_{0b}(x,t) \end{aligned} \quad (22)$$

The spring constant of the Winkler and the shear constant of the Pasternak type have been shown with K_w and K_G, respectively, C_d shows the visco type (Amir *et al*. 2020a, b).

5.3.2 Thermal load

External work not only includes the elastic environment but also, consists of thermal load in this structure (Arshid *et al*. 2020b)

$$W_2 = \int_0^A\left[\frac{1}{2N_T\left(\frac{\partial}{\partial x}w_i(x,z,t)\right)^2}\right]dAi = t,b,c \quad (23)$$

N_T is external work, leads to the thermal load in the

environment that has been shown in the following relation (Amir *et al*. 2019a)

$$N_T = \alpha(T)\Delta T\left(\int_{-\frac{h_t}{2}}^{\frac{h_t}{2}} E(z)dz + \int_{-\frac{h_c}{2}}^{\frac{h_c}{2}} E(z)dz + \int_{-\frac{h_b}{2}}^{\frac{h_b}{2}} E(z)dz\right) \quad (24)$$

$\alpha(T)$ and $E(z)$ are the temperature-dependent properties of the materials which are called thermal expansion and modulus of elasticity, respectively. ΔT is the temperature changes from the ambient (Fu *et al*. 2012).

6. Governing equations

As mentioned about HSAPT, the theory applied in sandwich beam includes 27 unknowns, which 19 unknowns are related to displacements and 8 equations are to Lagrangian coefficients. So, 27 equations are needed that include the following equations (Moradi-Dastjerdi and Malek-mohammadi 2016):

- 6 displacement equations for the top piezoelectric facesheets.
- 6 displacement equations for the bottom piezoelectric facesheets.
- 7 displacement equations for the honeycomb core.
- 4 equations for the interlayer continuum condition at the top and bottom layers.
- 2 equations for zero shear stress condition on top and bottom surfaces
- 2 equations for the condition of continuity of shear stress between layers.

The 27 main equations for sandwich beams include the PD controller and temperature load, are derived using the Hamilton's principle, in the "Appendix".

7. Analytical solution

Navier's solution method is used to obtain the results in beams containing simply supported boundary conditions of two sides, Eq. (26) is given to satisfy the geometric boundary conditions of the displacement field (Ghorbanpour Arani *et al*. 2016a, b)

$$\begin{aligned}
\lambda_x{}^t(x,t) &= \sum_{m=1}^{M} \lambda_x{}^t \cos\left(\frac{m\pi x}{L}\right) e^{i\omega t} \\
\lambda_x{}^b(x,t) &= \sum_{m=1}^{M} \lambda_x{}^b \cos\left(\frac{m\pi x}{L}\right) e^{i\omega t} \\
\lambda_z{}^t(x,t) &= \sum_{m=1}^{M} \lambda_z{}^t \sin\left(\frac{m\pi x}{L}\right) e^{i\omega t} \\
\lambda_z{}^b(x,t) &= \sum_{m=1}^{M} \lambda_z{}^b \sin\left(\frac{m\pi x}{L}\right) e^{i\omega t} \\
\lambda_{xz}{}^t(x,t) &= \sum_{m=1}^{M} \lambda_{xz}{}^t \cos\left(\frac{m\pi x}{L}\right) e^{i\omega t}
\end{aligned} \quad (25a)$$

$$\begin{aligned}
\lambda_{xz}{}^b(x,t) &= \sum_{m=1}^{M} \lambda_{xz}{}^b \cos\left(\frac{m\pi x}{L}\right) e^{i\omega t} \\
\lambda_{xz}{}^{tc}(x,t) &= \sum_{m=1}^{M} \lambda_{xz}{}^{tc} \cos\left(\frac{m\pi x}{L}\right) e^{i\omega t} \\
\lambda_{xz}{}^{bc}(x,t) &= \sum_{m=1}^{M} \lambda_{xz}{}^{bc} \cos\left(\frac{m\pi x}{L}\right) e^{i\omega t}
\end{aligned} \quad (25a)$$

$$\begin{aligned}
u_{0I}(x,t) &= \sum_{m=1}^{M} u_{0I} \cos\left(\frac{m\pi x}{L}\right) e^{i\omega t} \\
u_{1I}(x,t) &= \sum_{m=1}^{M} u_{1I} \cos\left(\frac{m\pi x}{L}\right) e^{i\omega t} \\
u_{2I}(x,t) &= \sum_{m=1}^{M} u_{2I} \cos\left(\frac{m\pi x}{L}\right) e^{i\omega t} \\
u_{3I}(x,t) &= \sum_{m=1}^{M} u_{3I} \cos\left(\frac{m\pi x}{L}\right) e^{i\omega t} \\
w_{0I}(x,t) &= \sum_{m=1}^{M} w_{0I} \sin\left(\frac{m\pi x}{L}\right) e^{i\omega t} \\
w_{1J}(x,t) &= \sum_{m=1}^{M} w_{1J} \sin\left(\frac{m\pi x}{L}\right) e^{i\omega t} \\
w_{2J}(x,t) &= \sum_{m=1}^{M} w_{2J} \sin\left(\frac{m\pi x}{L}\right) e^{i\omega t} \\
\varphi_s(x,t) &= \sum_{m=1}^{M} \varphi_s \sin\left(\frac{m\pi x}{L}\right) e^{i\omega t} \\
\varphi_a(x,t) &= \sum_{m=1}^{M} \varphi_a \sin\left(\frac{m\pi x}{L}\right) e^{i\omega t} \\
(I = t,b,c),&\quad (J = c)
\end{aligned} \quad (25b)$$

m is the axial wave number (Mokhtar *et al*. 2018). Placing functions of Eq. (26) in the equations of motion in order to analysis of vibrations gives the matrices (27). Therefore, the governing equations can be expressed in the following matrix (Ezzat *et al*. 2017)

$$([K] + i\omega[C] - \omega^2[M])\{X\} = 0 \quad (26)$$

Obtaining the eigenvalues of Eq. (26) gives the natural frequency of the beam. The stiffness, mass, and damping matrixes are shown with $[K]$, $[M]$ and $[C]$, respectively.

$$\begin{aligned}
\{X\} = \{&U_{0t}U_{1t}U_{2t}U_{3t}W_{0t}\varphi_s\lambda_x{}^t\lambda_z{}^t\lambda_{xz}{}^t\lambda_{xz}{}^{tc} \\
&U_{0c}U_{1c}U_{2c}U_{3c}W_{0c}W_{1c}W_{2c} \\
&U_{0b}U_{1b}U_{2b}U_{3b}W_{0b}\varphi_a\lambda_x{}^b\lambda_z{}^b\lambda_{xz}{}^b\lambda_{xz}{}^{bc}\}^T
\end{aligned} \quad (27)$$

8. Results and discussion

The material properties of the facesheet are listed in Table 1. The honeycomb core material and the facesheets are made of Aluminum (E = 70 GPa, ν = 0.3, ρ = 2702 kg/m^3) and PZT4, respectively. In order to validate this

theory, a three layered sandwich beam with simply supported boundary conditions with a homogenous core is considered, (E_c = 113.8 GPa, ν_c = 0.4, ρ_c = 4430 kg/m^3) and the facesheets includes composite reinforced by uniformly distributed carbon nanotubes (E_{11CNT} = 5.64 TPa, E_{22CNT} = 7.08 TPa, G_{12CNT} = 1.94 TPa, V_{NT} = 0.12, E_m = 2.5 GPa), the dimensionless natural frequency is defined as $\omega_1 = \omega l\sqrt{I_0/C_{111}}$, thus the results are shown in Table 2. This table shows the errors of achieved results in this theory are limited. Noteworthy, the slight difference between the results can be due to differences in displacement field theories used by Chen *et al*. (2016) and Wu *et al*. (2015) and the present study and also, the different approaches used to solve the differential equations. Therefore, the results and their accuracy are verified.

The effect of first-order shear deformation (FSD) theory with shear correction factor 5/6 and present theory, with various voltages to length-to-thickness ratio on dimension-less natural frequency is obtained in Fig. 3 (Xie *et al*. 2019). As it is seen in this table, the higher order theory includes the interlaminar stress continuity and interface stress at the core; it means; this theory is close to real conditions. This figure shows if the structure became longer, the results of two theories are becoming closer and the frequency decreases, too.

Table 1 Material properties of facesheets (PZT4) and (PZT5) (Amir *et al*. 2018, Ebrahimi and Jafari 2016)

Properties	PZT5	PZT4
$C_{11}(GPa)$	60.6	81.6
$C_{55}(GPa)$	25.6	23
$\alpha_{11}(K^{-1})$	0.2e-6	0.2e-6
$\rho(kg/m^3)$	7500	7500
$e_{31}(c/m^2)$	-16.6	-10
$e_{15}(c/m^2)$	44.9046	40.3248
$k_{11}(c^2/m^2N)$	1.5027e-8	0.6712e-8
$k_{33}(c^2/m^2N)$	2.554e-8	1.0275e-8

Table 2 Comparison of the nondimensional natural frequencies for a simple sandwich beam with the results of previous works (Chen *et al*. 2016, Wu *et al*. 2015)

Refs.	Mode 1	Mode 2	Mode 3
Chen et al. (2016) (Timoshenko Beam Theory & Ritz method Solution)	0.1453	0.5730	1.2599
Wu *et al*. (2015) (Timoshenko Beam Theory & DQ method Solution)	0.1453	0.5730	1.2599
Present (IHSAPT & Navier Solution)	0.1373	0.5538	1.2490
Present (Timoshenko Beam Theory & Navier Solution)	0.1376	0.5436	1.2389

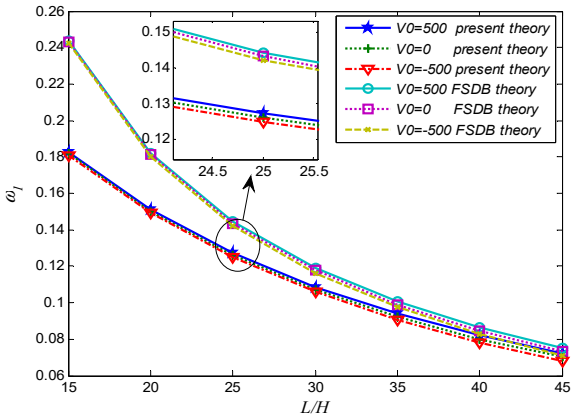

Fig. 3 Comparison of first order shear deformation theory with high order sandwich theory in terms of dimensionless frequency

The nondimensional frequency versus core to facesheets thickness ratio is shown in Fig. 4 for honeycomb, foam and porous with uniform porosity distributions and porosity coefficient 0.2. The porous material and honeycomb structure are two types of solid foams that their differences are about the way of productions and dispersion and shapes of cells. A comparison of the mechanical properties of the three mentioned materials is given below

$$E_{c(Foam)} > E_{c(honeycomb)} > E_{c(porous)}$$
$$\rho_{c(Foam)} = \rho_{c(porous)} \geq \rho_{c(honeycomb)}$$
$$\nu_{c(honeycomb)} > \nu_{c(porous)} = \nu_{c(foam)}$$
$$\xrightarrow[\omega \propto E_c \quad \omega \propto 1/\rho_c]{\omega \propto 1/\nu_c} \omega_{(Foam)} > \omega_{(honeycomb)} > \omega_{(porous)}$$

As the Fig. 4 shows, by increasing the core to facesheet dimensions ratio, the dimensionless frequency increases. In Fig. 5 the effect of three types of various materials for top and bottom structure is obtained, too. The PZT4 material is stiffer than others and causes the frequency of the structure become more. The properties of materials are shown in Tables 1-3.

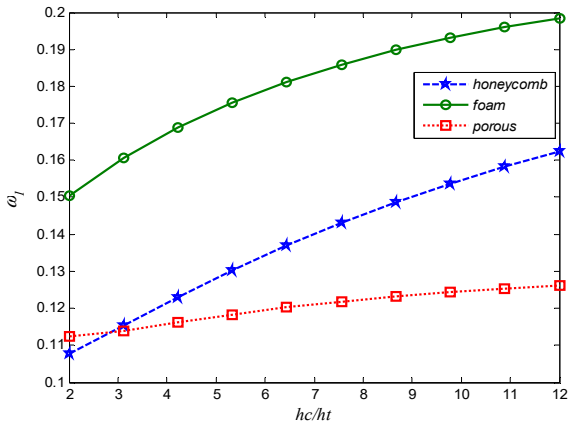

Fig. 4 Dimensionless frequency distribution in terms of core to facesheet thickness ratio for different core materials

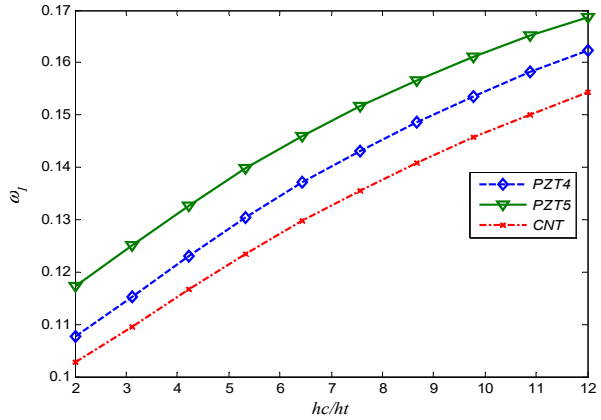

Fig. 5 Dimensionless frequency distribution in terms of core to facesheet thicknesses ratio

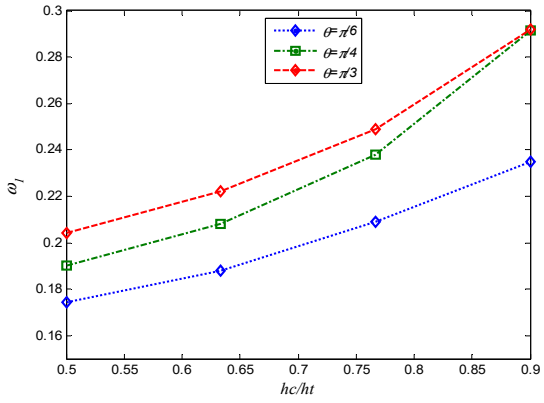

(a)

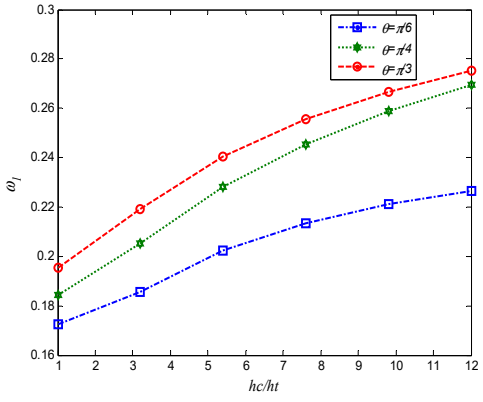

(b)

Fig. 6 (a) The effect of the internal angle ratio of the cells on the core to thickness ratio versus dimensionless frequency for total thickness is constant; (b) The effect of the internal angle ratio of the cells on the core to thickness ratio versus dimensionless frequency for the surface thickness is constant

Fig. 6 indicates the effects of cell angle at the honeycomb cells on the nondimensional frequency for three type core to facesheet thickness ratio. As it can be seen by increasing cell angle, the frequency increases, too, at the same time, the corresponding dimensionless natural frequencies increase as the core-to-surface ratio increases.

Table 3 Mechanical properties of Poly methyl methacrylate (PMMA) and single-walled carbon nanotube (SWCNT) facesheets (Mohammadimehr and Mostafavifar 2016, Arshid *et al*. 2021)

PMMA		SWCNT	
E_m (GPa)	2.5	E_{11CNT} (GPa)	5.6466
ρ_m (kg/m^3)	1190	E_{22CNT} (GPa)	7.0800
υ_m	0.3	G_{12CNT} (GPa)	1.9445
		ρ_{CNT} (kg/m^3)	1400
		υ_{CNT}	0.175

In Fig. 6(b), the ratio of thickness increases as the thickness of the core increases, but the thickness of the surfaces is constant. The length of the structure is $L = 15\ H$. Fig. 6(a), shows the total thickness is constant, while the core thickness increases and the surface thickness is decreasing. This graph shows that the honeycomb core has more effect on structural rigidity. These figures are in these conditions, $h_0 = l$, $\gamma_0 = 0.1$ and $\varphi_0 = 1$.

In Fig. 7, the effect of cell angle in the honeycomb core to the dimensionless frequency is shown by the thickness changes of the honeycomb cells. It can be understood, as

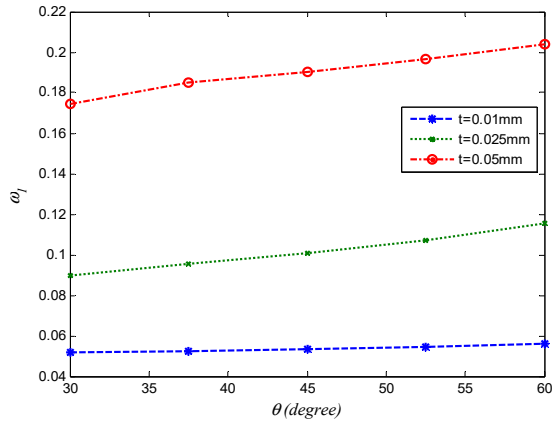

Fig. 7 The effect of honeycomb cell thickness on the cell angle versus nondimensional frequency

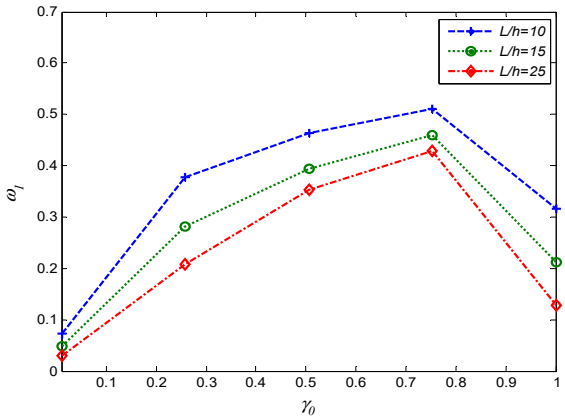

Fig. 8 Influence of the length-to-thickness ratio on the coefficient γ_0 versus the dimensionless frequency

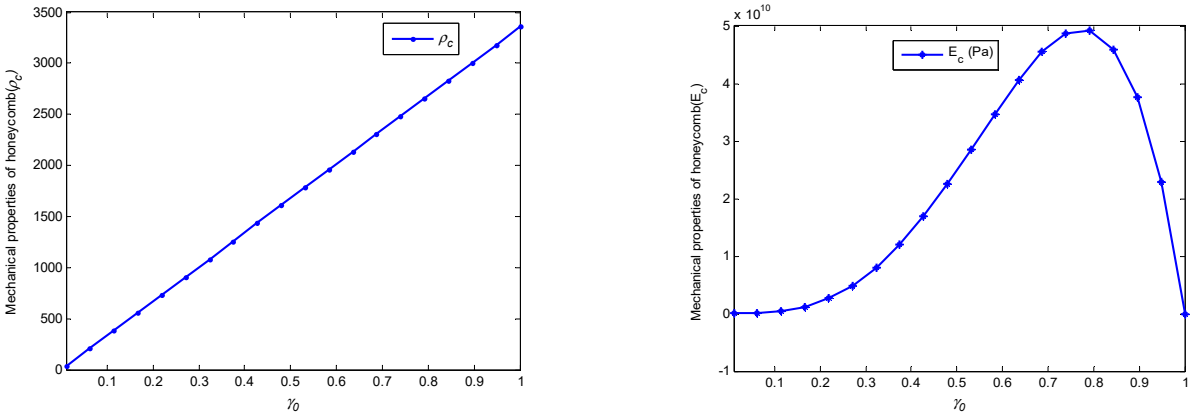

(a) (b)

Fig. 9 Influence of mechanical properties versus coefficient γ_0 for honeycomb core

the thickness of the cells increases, the first dimensionless frequency of the structure increases, also it can be justified, by increasing the thickness of t, the stiffness of the core increases, and as a result the frequency increases.

The effect of the coefficient γ_0 on the first nondimensional frequency is seen in the Fig. 8. At first, the chart trend is increasing and then decreases. The reason is that by increasing the coefficient γ_0 which is the $\frac{t_0}{l}$ ratio, the effect of the thickness is greater than the effect of l_0, so the stiffness of the structure increases. But after the value γ_0 = 0.8 according to Eq. (14), the density of the structure exceeds its stiffness and, as a result, the frequency decreases, which the mechanical properties of the elasticity modulus and density are shown in Fig. 9.

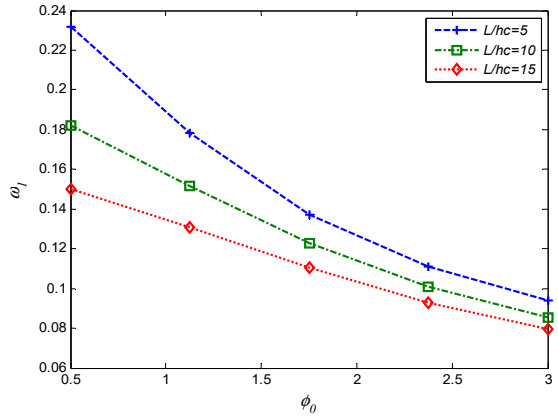

Fig. 10 Effects of internal aspect ratio of core's cells versus dimensionless frequency for different length-to-core thickness ratio

In Fig. 10 for three cases of the length-to-core thickness ratio of the sandwich beam, the dimensionless frequency variations are plotted in terms of the internal aspect ratio of the core (φ_0). This graph shows that as the length to core ratio is increasing, the nondimensional frequency of the beam decreases. The reason for this is that as the ratio increases, the structural stiffness decreases and on the other hand, its inertia increases. To prove this figure, in Fig. 11 the mechanical properties of honeycomb structure versus internal aspect ratio have been shown. As the internal aspect ratio increases, the modulus value and the density of the structure decrease. The reduction in the elastic modulus is much greater than the density. So, according to the equation between frequency, density and elasticity modulus, the core frequency decreases with honeycomb structure. But in

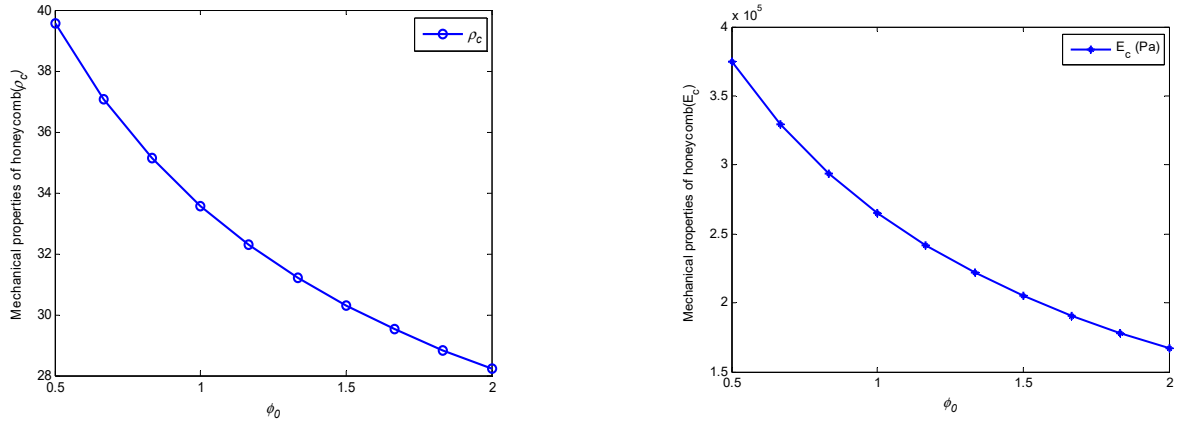

(a) (b)

Fig. 11 Effects of mechanical properties. (a) Elasticity modulus; (b) Density of core versus internal coefficient

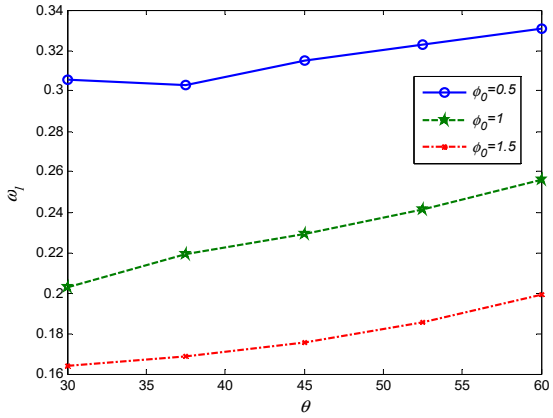

Fig. 12 Effect of internal coefficient on internal angle ratio of cell versus dimensionless frequency

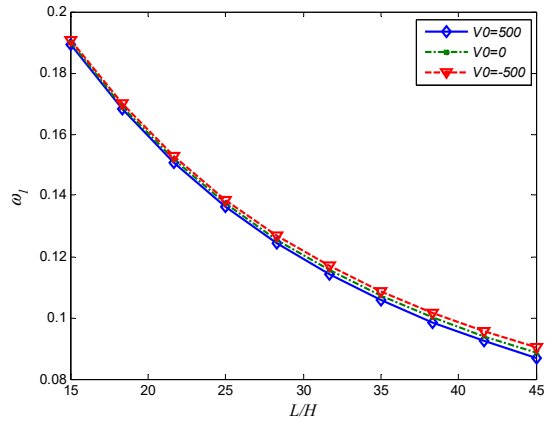

Fig. 13 Effects of voltage parameter and length to total thickness ratio on the dimensionless frequency of the system

plates by increasing this internal aspect ratio, the frequency increases too. Another result of this chart is that by increasing the φ_0, thicker beams, give the lower frequency.

Fig. 12 displays the variations of internal aspect ratio and internal angle of honeycomb cell versus nondimensional frequency. It can be understood, by increasing internal angle and decreasing internal aspect ratio, the first nondimensional frequency of the sandwich beam increased that the effect of the internal aspect ratio is more than the internal angle, on the trend of the chart.

The effect of the electric voltage applied on the actuator layer for the length to thickness ratio and various temperatures versus the frequency indicated in Figs. 13-14. It's clear that by applying a positive voltage, the frequency of the structure decreases. The reason for this trend is the production of pressure forces due to the positive voltage and tensile forces because of the negative voltage applied to the actuator layer. In addition, the applied voltage is more effective in a longer beam structure. The initial temperature is 300 Kelvin.

The influence of the spring and shear coefficient for the first nondimensional frequency, in terms of the damping coefficient, is shown in Fig. 15. By considering the effects of the elastic environment, as can be seen, the structural rigidity increases. It means the dimensionless frequency of the sandwich beam, when placed in the elastic medium, is higher than the sandwich beam without the elastic medium. As the effect of the damper environment on the sandwich beam increases, the frequency of the system decreases, conversely. Damping coefficient is a factor in the loss of system energy and assuming a visco environment, more energy is lost and the frequency is reduced. Therefore, it can be said that the viscoelastic environment coefficients have an important role in the vibrational behavior of the structures, and for more realistic modeling of structures, it is necessary to consider the environment around the structure.

The first dimensionless frequency to the length to thickness ratio is given in Fig. 16 in terms of different values of proportional and derivative control coefficients. And in Fig. 17 the values of these proportional and derivative coefficients are compared at the same time. As shown in Fig. 16, the frequency of the structure can be reduced or increased by considering the PD controller, and the control coefficients can be used with a proportional value depending on the application of the frequency. If the sandwich beam is thicker, the frequency changes with the controller are more noticeable. In both figures, it can be

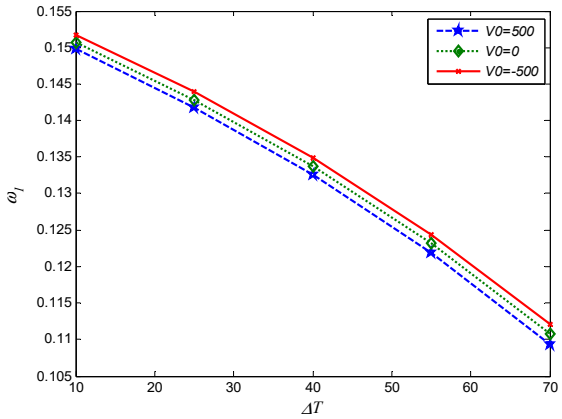

Fig. 14 Effects of temperature changes and different voltages versus dimensionless frequency

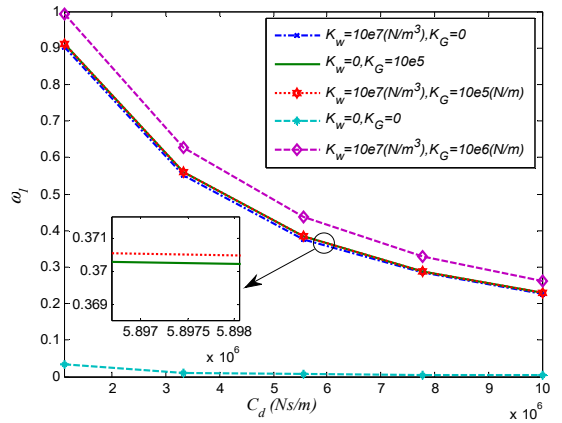

Fig. 15 Effects of Winkler coefficient and shear coefficient on first nondimensional frequency versus visco coefficient

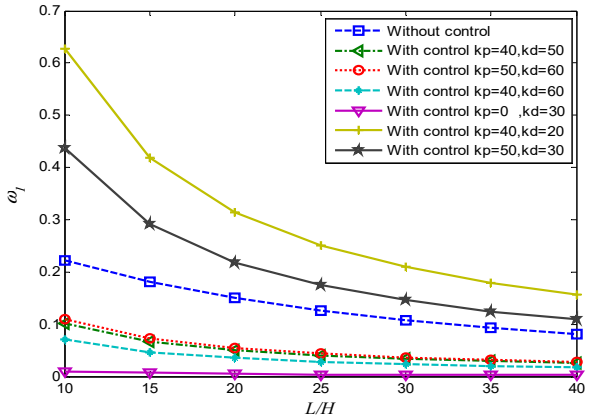

Fig. 16 Effects of controllers on the nondimensional frequency

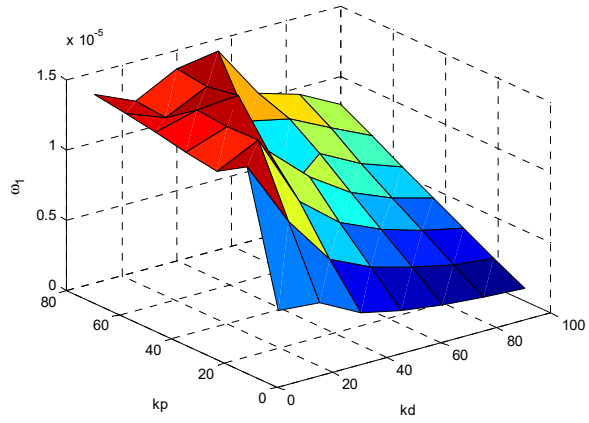

Fig. 17 Three-dimensional graph of derivative and proportional coefficients on first nondimensional frequency

concluded the proportional controller increases the frequency, but the derivative controller reduces the frequency, conversely. Another interesting result in this figure is the derivative controller is better than the PD controller because it reduces the frequency of the system more. Of course, just the derivative controller is not functional and cannot be used, because the derivative controller operates on the error signal changing rate. These diagrams are plotted without a visco-elastic environment.

9. Conclusions

The current study is aimed to analyze vibrations of a three-layered sandwich beam with a honeycomb core made of aluminum and PZT4 piezoelectric face sheets and presented a higher-order beam theory. The piezoelectric face sheets are affected by the PD controller, which can be effective on the frequencies. The structure is also placed in a thermal and viscoelastic environment. The main novelties of the present research lay in the displacement continuity equations at the interfaces. This type of honeycomb structure with the PD controller and by using this displacement theory had been never investigated. The findings of this work will help to design and create more optimal engineering and smart structures such as sensors and actuators, as well as the honeycomb structures due to the light constructions, are applied in air vehicles. The motion equations are derived by the IHSAPT and also temperature load and electric field are considered. Navier's analytical method is used to solve the governing equations. The following results can be obtained from this work:

- The natural frequencies of the beam increase with increasing thickness of the honeycomb core to the thickness of the piezoelectric layers. Also, by increasing the internal aspect ratio of honeycomb core, the frequency of the sandwich beam decreases; conversely, by increasing the internal angle ratio of the honeycomb cell, the frequency increases, which can be justified by the mechanical formulation used for the honeycomb core.
- The geometry of hexagonal cells has a significant effect on natural frequencies in the honeycomb core, and also the thickness of the honeycomb core has an important effect on natural frequencies.
- By applying a positive voltage to the actuator layer, the frequency of the system is reduced, due to the production of compressive and tensile forces, by applying positive and negative voltage, respectively, to the actuator layer of the system. Thus, the external voltage is an effective parameter in controlling the system.
- The derivative controller reduces system frequency but the proportional controller increases system frequency.
- In this project, by applying a PD controller, the system frequency can be increased or decreased compared to the uncontrolled state, that it depends on the application of the sandwich structure, which can be used the appropriate proportional and derivative coefficients.
- As the temperature and the length of the sandwich beam increasing, the system frequency decreases, because it reduces the rigidity and elasticity modulus of the beam.

Acknowledgments

The authors would like to thank the reviewers for their valuable comments and suggestions to improve the clarity of this study.

Funding

The authors are thankful to the University of Kashan for supporting this work by Grant No. 988099/6.

References

Abazid, M.A. and Sobhy, M. (2018), "Thermo-electro-mechanical bending of FG piezoelectric microplates on Pasternak foundation based on a four-variable plate model and the

modified couple stress theory", *Microsyst. Technol.*, **24**(2), 1227-1245. https://doi.org/10.1007/s00542-017-3492-8

AkhavanAlavi, S.M., Mohammadimehr, M. and Edjtahed, S.H. (2019), "Active control of micro Reddy beam integrated with functionally graded nanocomposite sensor and actuator based on linear quadratic regulator method", *Eur. J. Mech., A/Solids*, **74**, 449-461. https://doi.org/10.1016/j.euromechsol.2018.12.008

Amir, S., Khorasani, M. and BabaAkbar-Zarei, H. (2018), "Buckling analysis of nanocomposite sandwich plates with piezoelectric face sheets based on flexoelectricity and first-order shear deformation theory", *J. Sandw. Struct. Mater.*, **22**(7), 2186-2209. https://doi.org/10.1177/1099636218795385

Amir, S., Soleimani-Javid, Z. and Arshid, E. (2019), "Size-dependent free vibration of sandwich micro beam with porous core subjected to thermal load based on SSDBT", *ZAMM Zeitschrift Fur Angewandte Mathematik Und Mechanik*, **99**(9), 1-21. https://doi.org/10.1002/zamm.201800334

Amir, S., Arshid, E. and Khoddami Maraghi, Z. (2020a), "Free vibration analysis of magneto-rheological smart annular three-layered plates subjected to magnetic field in viscoelastic medium", *Smart Struct. Syst., Int. J.*, **25**(5), 581-592. https://doi.org/10.12989/sss.2020.25.5.581

Amir, S., Arshid, E., Khoddami Maraghi, Z., Loghman, A. and Ghorbanpour Arani, A. (2020b), "Vibration analysis of magnetorheological fluid circular sandwich plates with magnetostrictive facesheets exposed to monotonic magnetic field located on visco-Pasternak substrate", *J. Vib. Control*, **26**(17-18), 1523-1537. https://doi.org/10.1177/1077546319899203

Arefi, M. and Zenkour, A.M. (2017), "Thermo-electro-mechanical bending behavior of sandwich nanoplate integrated with piezoelectric face-sheets based on trigonometric plate theory", *Compos. Struct.*, **162**, 108-122. https://doi.org/10.1016/j.compstruct.2016.11.071

Arshid, E. and Khorshidvand, A.R. (2018), "Free vibration analysis of saturated porous FG circular plates integrated with piezoelectric actuators via differential quadrature method", *Thin-Wall. Struct.*, **125**, 220-233. https://doi.org/10.1016/j.tws.2018.01.007

Arshid, E., Khorshidvand, A.R. and Khorsandijou, S.M. (2019), "The effect of porosity on free vibration of SPFG circular plates resting on visco-Pasternak elastic foundation based on CPT, FSDT and TSDT", *Struct. Eng. Mech., Int. J.*, **70**(1), 97-112. https://doi.org/10.12989/sem.2019.70.1.097

Arshid, E., Amir, S. and Loghman, A. (2020a), "Bending and buckling behaviors of heterogeneous temperature-dependent micro annular/circular porous sandwich plates integrated by FGPEM nano-Composite layers", *J. Sandw. Struct. Mater.*, 109963622095502. https://doi.org/10.1177/1099636220955027

Arshid, E., Amir, S. and Loghman, A. (2020b), "Static and dynamic analyses of FG-GNPs reinforced porous nanocomposite annular micro-plates based on MSGT", *Int. J. Mech. Sci.*, **180**, 105656. https://doi.org/10.1016/j.ijmecsci.2020.105656

Arshid, E., Arshid, H., Amir, S. and Mousavi, S.B. (2021), "Free vibration and buckling analyses of FG porous sandwich curved microbeams in thermal environment under magnetic field based on modified couple stress theory", *Arch. Civil Mech. Eng.*, **21**(1), 6. https://doi.org/10.1007/s43452-020-00150-x

Chen, D., Kitipornchai, S. and Yang, J. (2016), "Nonlinear free vibration of shear deformable sandwich beam with a functionally graded porous core", *Thin-Wall. Struct.*, **107**, 39-48. https://doi.org/10.1016/J.TWS.2016.05.025

Cheng, S., Qiao, P., Chen, F., Fan, W. and Zhu, Z. (2016), "Free vibration analysis of fiber-reinforced polymer honeycomb sandwich beams with a refined sandwich beam theory", *J. Sandw. Struct. Mater.*, **18**(2), 242-260. https://doi.org/10.1177/1099636215619841

Dariushi, S. and Sadighi, M. (2015), "Analysis of composite sandwich beam with enhanced nonlinear high order sandwich panel theory", *Modares Mech. Eng.*, **14**(16), 1-8.

Ebrahimi, F. and Daman, M. (2017), "Nonlocal thermo-electro-mechanical vibration analysis of smart curved FG piezoelectric Timoshenko nanobeam", *Smart Struct. Syst, Int. J.*, **20**(3), 351-368. https://doi.org/10.12989/sss.2017.20.3.351

Ebrahimi, F. and Jafari, A. (2016), "Thermo-mechanical vibration analysis of temperature-dependent porous FG beams based on Timoshenko beam theory", *Struct. Eng. Mech., Int. J.*, **59**(2), 343-371. https://doi.org/10.12989/sem.2016.59.2.343

Ezzat, M.A., El Karamany, A.S. and El-Bary, A.A. (2017), "Thermoelectric viscoelastic materials with memory-dependent derivative", *Smart Struct. Syst., Int. J.*, **19**(5), 539-551. https://doi.org/10.12989/sss.2017.19.5.539

Fallah, N. and Ebrahimnejad, M. (2014), "Finite volume analysis of adaptive beams with piezoelectric sensors and actuators", *Appl. Mathe. Modell.*, **38**(2), 722-737. https://doi.org/10.1016/j.apm.2013.07.004

Frostig, Y. and Thomsen, O.T. (2004), "High-order free vibration of sandwich panels with a flexible core", *Int. J. Solids Struct.*, **41**, 1697-1724. https://doi.org/10.1016/j.ijsolstr.2003.09.051

Frostig, Y., Baruch, M., Vilnay, O. and Sheinman, I. (1992), "High-order theory for sandwich-beam behavior with transversely flexible core", *J. Eng. Mech.*, **118**(5), 1026-1043. https://doi.org/10.1061/(ASCE)0733-9399(1992)118:5(1026)

Fu, M. and Yin, J. (1999), "Equivalent elastic parameters of the honeycomb core", *Acta Mechanica Sinica*, **15**(1), 113-118.

Fu, Y., Wang, J. and Mao, Y. (2012), "Nonlinear analysis of buckling, free vibration and dynamic stability for the piezoelectric functionally graded beams in thermal environment", *Appl. Mathe. Modell.*, **36**(9), 4324-4340. https://doi.org/10.1016/j.apm.2011.11.059

Ghorbanpour Arani, A., Jafari, G.S. and Kolahchi, R. (2016a), "Vibration analysis of nanocomposite microplates integrated with sensor and actuator layers using surface SSDPT", **39**(6), 1-14. https://doi.org/10.1002/pc.24150

Ghorbanpour Arani, A., Arani, H.K. and Maraghi, Z.K. (2016b), "Vibration analysis of sandwich composite micro-plate under electro-magneto-mechanical loadings", *Appl. Mathe. Modell.*, **40**(23-24), 10596-10615. https://doi.org/10.1016/j.apm.2016.07.033

Ghorbanpour Arani, A., BabaAkbar Zarei, H. and Haghparast, E. (2018), "Vibration response of viscoelastic sandwich plate with magnetorheological fluid core and functionally graded-piezoelectric nanocomposite face sheets", *J. Vib. Control*, **24**(21), 17-21. https://doi.org/10.1177/1077546317747501

Hadji, L. (2017), "Analysis of functionally graded plates using a sinusoidal shear deformation theory", *Smart Struct. Syst, Int. J.*, **19**(4), 441-448. https://doi.org/10.12989/sss.2017.19.4.441

Hong, C.C. (2013), "Thermal vibration of magnetostrictive functionally graded material shells", *Eur. J. Mech. A/Solids*, **40**, 114-122. https://doi.org/10.1016/j.euromechsol.2013.01.010

Jedari Salami, S., Dariushi, S., Sadighi, M. and Shakeri, M. (2016), "An advanced high-order theory for bending analysis of moderately thick faced sandwich beams", *Eur. J. Mech. A/Solids*, **56**, 1-11. https://doi.org/10.1016/j.euromechsol.2015.10.003

Khalili, S.M.R., Kheirikhah, M.M. and Fard, K.M. (2013), "Biaxial wrinkling analysis of composite-faced sandwich plates with soft core using improved high-order theory", *Eur. J. Mech. A/Solids*, **43**, 68-77. https://doi.org/10.1016/j.euromechsol.2013.08.002

Kheirikhah, M.M., Khalili, S.M.R. and Fard, K.M. (2012a), "Biaxial buckling analysis of soft-core composite sandwich plates using improved high-order theory", *Eur. J. Mech.*

A/*Solids*, **31**(1), 54-66. https://doi.org/10.1016/j.euromechsol.2011.07.003

Kheirikhah, M.M., Khalili, S.M.R. and Malekzadeh Fard, K. (2012b), "Analytical solution for bending analysis of soft-core composite sandwich plates using improved high-order theory", *Struct*. *Eng*. *Mech*., *Int*. *J*., **44**(1), 15-34. https://doi.org/10.12989/sem.2012.44.1.015

Lorna, J. and Gibson, M.F.A. (1989), "Cellular solids", *J*. *Biomech*. https://doi.org/10.1016/0021-9290(89)90056-0

Malekzadeh, K., Khalili, M.R. and Mittal, R.K. (2005), "Local and global damped vibrations of plates with a viscoelastic soft flexible core: An improved high-order approach", *J*. *Sandw*. *Struct*. *Mater*., **7**(5), 431-456. https://doi.org/10.1177/1099636205053748

Mohammadimehr, M. and Mostafavifar, M. (2016), "Free vibration analysis of sandwich plate with a transversely flexible core and FG-CNTs reinforced nanocomposite face sheets subjected to magnetic field and temperature-dependent material properties using SGT", *Compos*. *Part B*: *Eng*., **94**, 253-270. https://doi.org/10.1016/j.compositesb.2016.03.030

Mokhtar, Y., Heireche, H., Bousahla, A.A., Houari, M.S.A., Tounsi, A. and Mahmoud, S.R. (2018), "A novel shear deformation theory for buckling analysis of single layer graphene sheet based on nonlocal elasticity theory", *Smart Struct*. *Syst*., *Int*. *J*., **21**(4), 397-405. https://doi.org/10.12989/sss.2018.21.4.397

Moradi-Dastjerdi, R. and Malek-Mohammadi, H. (2016), "Biaxial buckling analysis of functionally graded nanocomposite sandwich plates reinforced by aggregated carbon nanotube using improved high-order theory", *J*. *Sandw*. *Struct*. *Mater*., **19**(6), 736-769. https://doi.org/10.1177/1099636216643425

Moradi Dastjerdi, R., Payganeh, G., Rajabizadeh Mirakabad, S. and Jafari Mofrad-Taheri, M. (2016), "Static and free vibration analyses of functionally graded nano-composite plates reinforced by wavy carbon nanotubes resting on a Pasternak elastic foundation", *Mech*. *Adv*. *Compos*. *Struct*., **3**, 123-135. https://doi.org/10.22075/macs.2016.474

Nezami, M. and Gholami, B. (2015), "Active flutter control of a supersonic honeycomb sandwich beam resting on elastic foundation with piezoelectric sensor/actuator pair", *Int*. *J*. *Struct*. *Stabil*. *Dyn*., **15**(3), p. 1450052. https://doi.org/10.1142/s0219455414500527

Nguyen, H.X., Nguyen, T.N., Bordas, S.P.A. and Vo, T.P. (2016), "A refined quasi-3D isogeometric analysis for functionally graded microplates based on the modified couple stress theory", *Comput*. *Methods Appl*. *Mech*. *Eng*., **313**, 904-940. https://doi.org/10.1016/j.cma.2016.10.002

Nguyen, T.N., Ngo, T.D. and Nguyen-Xuan, H. (2017), "A novel three-variable shear deformation plate formulation: Theory and Isogeometric implementation", *Comput*. *Methods Appl*. *Mech*. *Eng*., **326**, 376-401. https://doi.org/10.1016/j.cma.2017.07.024

Nguyen, T.N., Thai, C.H., Luu, A.T., Nguyen-Xuan, H. and Lee, J. (2019), "NURBS-based postbuckling analysis of functionally graded carbon nanotube-reinforced composite shells", *Comput*. *Methods Appl*. *Mech*. *Eng*., **347**, 983-1003. https://doi.org/10.1016/j.cma.2019.01.011

Phung-Van, P., Lorenzis, L. De, Thai, C.H., Abdel-Wahab, M. and Nguyen-Xuan, H. (2015), "Analysis of laminated composite plates integrated with piezoelectric sensors and actuators using higher-order shear deformation theory and isogeometric finite elements", *Computat*. *Mater*. *Sci*., **96**, 495-505. https://doi.org/10.1016/j.commatsci.2014.04.068

Şakar, G. and Bolat, F.Ç. (2015), "The free vibration analysis of honeycomb sandwich beam using 3D and continuum model", *Int*. *J*. *Mech*. *Aerosp*. *Indust*. *Mechatron*. *Manuf*. *Eng*., **9**(6), 1077-1081.

Torabi, K., Afshari, H. and Aboutalebi, F.H. (2019), "Vibration and flutter analyses of cantilever trapezoidal honeycomb sandwich plates", *J*. *Sandw*. *Struct*. *Mater*., **21**(8), 2887-2920. https://doi.org/10.1177/1099636217728746

Wu, H., Kitipornchai, S. and Yang, J. (2015), "Free vibration and buckling analysis of sandwich beams with functionally graded carbon nanotube-reinforced composite face sheets", *Int*. *J*. *Struct*. *Stabil*. *Dyn*., **15**(7), 1540011. https://doi.org/10.1142/S0219455415400118

Xie, K., Wang, Y., Fan, X. and Fu, T. (2019), "Nonlinear free vibration analysis of functionally graded beams by using different shear deformation theories", *Appl*. *Mathe*. *Modell*., **77**, 1860-1880. https://doi.org/10.1016/j.apm.2019.09.024

Yiqi, M. and Yiming, F. (2010), "Nonlinear dynamic response and active vibration control for piezoelectric functionally graded plate", *J*. *Sound Vib*., **329**(11), 2015-2028. https://doi.org/10.1016/j.jsv.2010.01.005

Yongqiang, L. and Dawei, Z. (2009), "Free flexural vibration analysis of symmetric rectangular honeycomb panels using the improved Reddy's third-order plate theory", *Compos*. *Struct*., **88**(1), 33-39. https://doi.org/10.1016/j.compstruct.2008.03.033

Yue, Y.M., Xu, K.Y. and Chen, T. (2016), "A micro scale Timoshenko beam model for piezoelectricity with flexoelectricity and surface effects", *Compos*. *Struct*., **136**, 278-286. https://doi.org/10.1016/j.compstruct.2015.09.046

Zhang, Z.J., Han, B., Zhang, Q.C. and Jin, F. (2017), "Free vibration analysis of sandwich beams with honeycomb-corrugation hybrid cores", *Compos*. *Struct*., **171**, 335-344. https://doi.org/10.1016/j.compstruct.2017.03.045

Zhang, R., Ni, Y.Q., Duan, Y. and Ko, J.M. (2019), "Development of a full-scale magnetorheological damper model for open-loop cable vibration control", *Smart Struct*. *Syst*., *Int*. *J*., **23**(6), 553-564. https://doi.org/10.12989/sss.2019.23.6.553

CC

Appendix A

δu_{0t}:

$$(I_{0t})\frac{\partial^2}{\partial t^2}u_{0t}(x,t)+(I_{1t})\frac{\partial^2}{\partial t^2}u_{1t}(x,t)+(I_{2t})\frac{\partial^2}{\partial t^2}u_{2t}(x,t)+(I_{3t})\frac{\partial^2}{\partial t^2}u_{3t}(x,t)-(C_{110t})\frac{\partial^2}{\partial x^2}u_{0t}(x,t)-(C_{111t})\frac{\partial^2}{\partial x^2}u_{1t}(x,t)$$
$$-(C_{112t})\frac{\partial^2}{\partial x^2}u_{2t}(x,t)-(C_{113t})\frac{\partial^2}{\partial x^2}u_{3t}(x,t)+{\lambda_x}^t(x,t)-F_{310t}\frac{\partial}{\partial x}\varphi_s(x,t)-E_{310t}\frac{\partial}{\partial x}\varphi_s(x,t)=0 \quad (A1)$$

δu_{0b}:

$$(I_{0b})\frac{\partial^2}{\partial t^2}u_{0b}(x,t)+(I_{1b})\frac{\partial^2}{\partial t^2}u_{1b}(x,t)+(I_{2b})\frac{\partial^2}{\partial t^2}u_{2b}(x,t)+(I_{3b})\frac{\partial^2}{\partial t^2}u_{3b}(x,t)-(C_{110b})\frac{\partial^2}{\partial x^2}u_{0b}(x,t)-(C_{111b})\frac{\partial^2}{\partial x^2}u_{1b}(x,t)$$
$$-(C_{112b})\frac{\partial^2}{\partial x^2}u_{2b}(x,t)-(C_{113b})\frac{\partial^2}{\partial x^2}u_{3b}(x,t)+{\lambda_x}^b(x,t)+\left(K_pF_{310b}\right)\frac{\partial}{\partial x}\varphi_s(x,t)-\left(K_pE_{310b}\right)\frac{\partial}{\partial x}\varphi_s(x,t) \quad (A2)$$
$$+(K_dF_{310b})\frac{\partial^2}{\partial x\partial t}\varphi_s(x,t)-(K_dE_{310b})\frac{\partial^2}{\partial x\partial t}\varphi_s(x,t)=0$$

δu_{0c}:

$$(I_{0c})\frac{\partial^2}{\partial t^2}u_{0c}(x,t)+(I_{1c})\frac{\partial^2}{\partial t^2}u_{1c}(x,t)+(I_{2c})\frac{\partial^2}{\partial t^2}u_{2c}(x,t)+(I_{3c})\frac{\partial^2}{\partial t^2}u_{3c}(x,t)-(C_{110c})\frac{\partial^2}{\partial x^2}u_{0c}(x,t)-(C_{111c})\frac{\partial^2}{\partial x^2}u_{1c}(x,t)$$
$$-(C_{112c})\frac{\partial^2}{\partial x^2}u_{2c}(x,t)-(C_{113c})\frac{\partial^2}{\partial x^2}u_{3c}(x,t)-{\lambda_x}^t(x,t)-{\lambda_x}^b(x,t)-2(C_{130c})\frac{\partial}{\partial x}w_{1c}(x,t)-2(C_{131c})\frac{\partial}{\partial x}w_{2c}(x,t)=0 \quad (A3)$$

δu_{1t}:

$$(I_{1t})\frac{\partial^2}{\partial t^2}u_{0t}(x,t)+(I_{2t})\frac{\partial^2}{\partial t^2}u_{1t}(x,t)+(I_{3t})\frac{\partial^2}{\partial t^2}u_{2t}(x,t)+(I_{4t})\frac{\partial^2}{\partial t^2}u_{3t}(x,t)-(C_{111t})\frac{\partial^2}{\partial x^2}u_{0t}(x,t)-(C_{112t})\frac{\partial^2}{\partial x^2}u_{1t}(x,t)$$
$$-(C_{113t})\frac{\partial^2}{\partial x^2}u_{2t}(x,t)-(C_{114t})\frac{\partial^2}{\partial x^2}u_{3t}(x,t)+(C_{550t})u_{1t}(x,t)+(C_{550t})\frac{\partial}{\partial x}w_{0t}(x,t)+2(C_{551t})u_{2t}(x,t)+3(C_{552t})u_{3t}(x,t) \quad (A4)$$
$$+\frac{h_t}{2}{\lambda_x}^t(x,t)+{\lambda_{xz}}^t(x,t)+{C_{55}}^t{\lambda_{xz}}^{tc}(x,t)-F_{311t}\frac{\partial}{\partial x}\varphi_s(x,t)-E_{311t}\frac{\partial}{\partial x}\varphi_s(x,t)-F_{150t}\frac{\partial}{\partial x}\varphi_s(x,t)+E_{150t}\frac{\partial}{\partial x}\varphi_s(x,t)=0$$

δu_{1b}:

$$(I_{1b})\frac{\partial^2}{\partial t^2}u_{0b}(x,t)+(I_{2b})\frac{\partial^2}{\partial t^2}u_{1b}(x,t)+(I_{3b})\frac{\partial^2}{\partial t^2}u_{2b}(x,t)+(I_{4b})\frac{\partial^2}{\partial t^2}u_{3b}(x,t)-(C_{111b})\frac{\partial^2}{\partial x^2}u_{0b}(x,t)$$
$$-(C_{112b})\frac{\partial^2}{\partial x^2}u_{1b}(x,t)-(C_{113b})\frac{\partial^2}{\partial x^2}u_{2b}(x,t)-(C_{114b})\frac{\partial^2}{\partial x^2}u_{3b}(x,t)+(C_{550b})u_{1b}(x,t)$$
$$+(C_{550b})\frac{\partial}{\partial x}w_{0b}(x,t)+2(C_{551b})u_{2b}(x,t)+3(C_{552b})u_{3b}(x,t)-\frac{h_b}{2}{\lambda_x}^b(x,t)+{\lambda_{xz}}^b(x,t)+{C_{55}}^b{\lambda_{xz}}^{bc}(x,t) \quad (A5)$$
$$+(K_dF_{311b})\frac{\partial^2}{\partial x\partial t}\varphi_s(x,t)-(K_dE_{311b})\frac{\partial^2}{\partial x\partial t}\varphi_s(x,t)+\left(K_pF_{311b}\right)\frac{\partial}{\partial x}\varphi_s(x,t)-\left(K_pE_{311b}\right)\frac{\partial}{\partial t}\varphi_s(x,t)$$
$$-2\left(K_pE_{150b}\right)\frac{\partial}{\partial x}\varphi_s(x,t)-2\left(K_pF_{150b}\right)\frac{\partial}{\partial x}\varphi_s(x,t)-2(K_dE_{150b})\frac{\partial^2}{\partial x\partial t}\varphi_s(x,t)-2(K_dF_{150b})\frac{\partial^2}{\partial x\partial t}\varphi_s(x,t)=0$$

δu_{1c}:

$$(I_{1c})\frac{\partial^2}{\partial t^2}u_{0c}(x,t)+(I_{2c})\frac{\partial^2}{\partial t^2}u_{1c}(x,t)+(I_{3c})\frac{\partial^2}{\partial t^2}u_{2c}(x,t)+(I_{4c})\frac{\partial^2}{\partial t^2}u_{3c}(x,t)-(C_{111c})\frac{\partial^2}{\partial x^2}u_{0c}(x,t)-(C_{112c})\frac{\partial^2}{\partial x^2}u_{1c}(x,t)$$
$$-(C_{113c})\frac{\partial^2}{\partial x^2}u_{2c}(x,t)-(C_{114c})\frac{\partial^2}{\partial x^2}u_{3c}(x,t)+(C_{550c})u_{1c}(x,t)+(C_{550c})\frac{\partial}{\partial x}w_{0c}(x,t)+2(C_{551c})u_{2c}(x,t)+3(C_{552c})u_{3c}(x,t) \quad (A6)$$
$$-\frac{h_c}{2}{\lambda_x}^b(x,t)+\frac{h_c}{2}{\lambda_x}^t(x,t)-{C_{55}}^c{\lambda_{xz}}^{tc}(x,t)-{C_{55}}^c{\lambda_{xz}}^{bc}(x,t)=0$$

δu_{2t}:

$$(I_{2t})\frac{\partial^2}{\partial t^2}u_{0t}(x,t)+(I_{3t})\frac{\partial^2}{\partial t^2}u_{1t}(x,t)+(I_{4t})\frac{\partial^2}{\partial t^2}u_{2t}(x,t)+(I_{5t})\frac{\partial^2}{\partial t^2}u_{3t}(x,t)-(C_{112t})\frac{\partial^2}{\partial x^2}u_{0t}(x,t)$$
$$-(C_{113t})\frac{\partial^2}{\partial x^2}u_{1t}(x,t)-(C_{114t})\frac{\partial^2}{\partial x^2}u_{2t}(x,t)-(C_{115t})\frac{\partial^2}{\partial x^2}u_{3t}(x,t)+2(C_{551t})u_{1t}(x,t)+2(C_{551t})\frac{\partial}{\partial x}w_{0t}(x,t) \quad (A7)$$
$$+4(C_{552t})u_{2t}(x,t)+6(C_{553t})u_{3t}(x,t)+\frac{{h_t}^2}{4}{\lambda_x}^t(x,t)-h_t{\lambda_{xz}}^t(x,t)+h_t{C_{55}}^t{\lambda_{xz}}^{tc}(x,t)-F_{312t}\frac{\partial}{\partial x}\varphi_s(x,t)$$
$$-E_{312t}\frac{\partial}{\partial x}\varphi_s(x,t)+2E_{151t}\frac{\partial}{\partial x}\varphi_s(x,t)-2F_{151t}\frac{\partial}{\partial x}\varphi_s(x,t)=0$$

δu_{2b}:

$$(I_{2b})\frac{\partial^2}{\partial t^2}u_{0b}(x,t)+(I_{3b})\frac{\partial^2}{\partial t^2}u_{1b}(x,t)+(I_{4b})\frac{\partial^2}{\partial t^2}u_{2b}(x,t)+(I_{5b})\frac{\partial^2}{\partial t^2}u_{3b}(x,t)-(C_{112b})\frac{\partial^2}{\partial x^2}u_{0b}(x,t)$$
$$-(C_{113b})\frac{\partial^2}{\partial x^2}u_{1b}(x,t)-(C_{114b})\frac{\partial^2}{\partial x^2}u_{2b}(x,t)-(C_{115b})\frac{\partial^2}{\partial x^2}u_{3b}(x,t)+2(C_{551b})u_{1b}(x,t)+2(C_{551b})\frac{\partial}{\partial x}w_{0b}(x,t)$$
$$+4(C_{552b})u_{2b}(x,t)+6(C_{553})u_{3b}(x,t)+\frac{{h_b}^2}{4}{\lambda_x}^b(x,t)-h_b{\lambda_{xz}}^b(x,t)+h_b{C_{55}}^b{\lambda_{xz}}^{bc}(x,t)+\left(K_pF_{312b}\right)\frac{\partial}{\partial x}\varphi_s(x,t) \quad \text{(A8)}$$
$$-\left(K_pE_{312b}\right)\frac{\partial}{\partial x}\varphi_s(x,t)-2\left(K_pE_{151b}\right)\frac{\partial}{\partial x}\varphi_s(x,t)-2\left(K_pF_{151b}\right)\frac{\partial}{\partial x}\varphi_s(x,t)-2(K_dF_{151b})\frac{\partial^2}{\partial x\partial t}\varphi_s(x,t)$$
$$-2(K_dE_{151b})\frac{\partial}{\partial x\partial t}\varphi_s(x,t)+(K_dF_{312b})\frac{\partial^2}{\partial t\partial x}\varphi_s(x,t)-(K_dE_{312b})\frac{\partial^2}{\partial t\partial x}\varphi_s(x,t)=0$$

δu_{2c}:

$$(I_{2c})\frac{\partial^2}{\partial t^2}u_{0c}(x,t)+(I_{3c})\frac{\partial^2}{\partial t^2}u_{1c}(x,t)+(I_{4c})\frac{\partial^2}{\partial t^2}u_{2c}(x,t)+(I_{5c})\frac{\partial^2}{\partial t^2}u_{3c}(x,t)-(C_{112c})\frac{\partial^2}{\partial x^2}u_{0c}(x,t)$$
$$-(C_{113c})\frac{\partial^2}{\partial x^2}u_{1c}(x,t)-(C_{114c})\frac{\partial^2}{\partial x^2}u_{2c}(x,t)-(C_{115c})\frac{\partial^2}{\partial x^2}u_{3c}(x,t)+2(C_{551b})u_{1b}(x,t)+2(C_{551b})\frac{\partial}{\partial x}w_{0b}(x,t)$$
$$+4(C_{552b})u_{2b}(x,t)+6(C_{553})u_{3b}(x,t)-\frac{{h_c}^2}{4}{\lambda_x}^t(x,t)-\frac{{h_c}^2}{4}{\lambda_x}^b(x,t)-h_c{C_{55}}^c{\lambda_{xz}}^{tc}(x,t)+h_c{C_{55}}^c{\lambda_{xz}}^{bc}(x,t) \quad \text{(A9)}$$
$$-(C_{132c})\frac{\partial}{\partial x}w_{1c}(x,t)+2(C_{133c})\frac{\partial}{\partial x}w_{2c}(x,t)+2(C_{552c})\frac{\partial}{\partial x}w_{1c}(x,t)+2(C_{553c})\frac{\partial}{\partial x}w_{2c}(x,t)=0$$

δu_{3t}:

$$(I_{3t})\frac{\partial^2}{\partial t^2}u_{0t}(x,t)+(I_{4t})\frac{\partial^2}{\partial t^2}u_{1t}(x,t)+(I_{5t})\frac{\partial^2}{\partial t^2}u_{2t}(x,t)+(I_{6t})\frac{\partial^2}{\partial t^2}u_{3t}(x,t)-(C_{113t})\frac{\partial^2}{\partial x^2}u_{0t}(x,t)$$
$$-(C_{114t})\frac{\partial^2}{\partial x^2}u_{1t}(x,t)-(C_{115t})\frac{\partial^2}{\partial x^2}u_{2t}(x,t)-(C_{116t})\frac{\partial^2}{\partial x^2}u_{3t}(x,t)+3(C_{552t})u_{1t}(x,t)+3(C_{552t})\frac{\partial}{\partial x}w_{0t}(x,t) \quad \text{(A10)}$$
$$+6(C_{553t})u_{2t}(x,t)+9(C_{554t})u_{3t}(x,t)+\frac{{h_t}^3}{8}{\lambda_x}^t(x,t)+\frac{3}{4}{h_t}^2{\lambda_{xz}}^t(x,t)+\frac{3}{4}{h_t}^2{C_{55}}^t{\lambda_{xz}}^{tc}(x,t)$$
$$-F_{313t}\frac{\partial}{\partial x}\varphi_s(x,t)-E_{311t}\frac{\partial}{\partial x}\varphi_s(x,t)+3E_{152t}\frac{\partial}{\partial x}\varphi_s(x,t)-3F_{152t}\frac{\partial}{\partial x}\varphi_s(x,t)=0$$

δu_{3c}:

$$(I_{3c})\frac{\partial^2}{\partial t^2}u_{0c}(x,t)+(I_{4c})\frac{\partial^2}{\partial t^2}u_{1c}(x,t)+(I_{5c})\frac{\partial^2}{\partial t^2}u_{2c}(x,t)+(I_{6c})\frac{\partial^2}{\partial t^2}u_{3c}(x,t)-(C_{113c})\frac{\partial^2}{\partial x^2}u_{0c}(x,t)$$
$$-(C_{114c})\frac{\partial^2}{\partial x^2}u_{1c}(x,t)-(C_{115c})\frac{\partial^2}{\partial x^2}u_{2c}(x,t)-(C_{116c})\frac{\partial^2}{\partial x^2}u_{3c}(x,t)+3(C_{552c})u_{1c}(x,t)$$
$$+3(C_{552c})\frac{\partial}{\partial x}w_{0c}(x,t)+6(C_{553c})u_{2c}(x,t)+9(C_{554c})u_{3c}(x,t)-\frac{{h_c}^3}{8}{\lambda_x}^b(x,t)+\frac{{h_c}^3}{8}{\lambda_x}^t(x,t) \quad \text{(A11)}$$
$$-\frac{3}{4}{C_{55}}^c{h_c}^2{\lambda_{xz}}^{tc}(x,t)-\frac{3}{4}{h_c}^2{C_{55}}^b{\lambda_{xz}}^{bc}(x,t)-(C_{133c})\frac{\partial}{\partial x}w_{1c}(x,t)+2(C_{134c})\frac{\partial}{\partial x}w_{2c}(x,t)$$
$$+3(C_{553c})\frac{\partial}{\partial x}w_{1c}(x,t)+3(C_{554c})\frac{\partial}{\partial x}w_{2c}(x,t)=0$$

δw_{0t}:

$$(I_{0t})\frac{\partial^2}{\partial t^2}w_{0t}(x,t)+(I_{1t})\frac{\partial^2}{\partial t^2}w_{1t}(x,t)+(I_{2t})\frac{\partial^2}{\partial t^2}w_{2t}(x,t)-(C_{550t})\frac{\partial}{\partial x}u_{1t}(x,t)-(C_{550t})\frac{\partial^2}{\partial x^2}w_{0t}(x,t)$$
$$-2(C_{551t})\frac{\partial}{\partial x}u_{2t}(x,t)-3(C_{552t})\frac{\partial}{\partial x}u_{3t}(x,t)+{\lambda_z}^t(x,t)-\frac{\partial}{\partial x}C_{55t}{\lambda_{xz}}^{tc}(x,t) \quad \text{(A12)}$$
$$-\frac{\partial}{\partial x}{\lambda_{xz}}^t(x,t)+F_{150t}\frac{\partial^2}{\partial x^2}\varphi_s(x,t)-E_{150t}\frac{\partial^2}{\partial x^2}\varphi_s(x,t)-\mathrm{N}_0\left(\frac{\partial^2}{\partial x^2}w_{0b}(x,t)\right)=0$$

δw_{0b}:

$$\begin{aligned}&(I_{0b})\frac{\partial^2}{\partial t^2}w_{0b}(x,t)+(I_{1b})\frac{\partial^2}{\partial t^2}w_{1b}(x,t)+(I_{2b})\frac{\partial^2}{\partial t^2}w_{2b}(x,t)-(C_{550b})\frac{\partial}{\partial x}u_{1b}(x,t)-(C_{550b})\frac{\partial^2}{\partial x^2}w_{0b}(x,t)\\&-2(C_{551b})\frac{\partial}{\partial x}u_{2b}(x,t)-3(C_{552b})\frac{\partial}{\partial x}u_{3b}(x,t)+{\lambda_z}^b(x,t)-\frac{\partial}{\partial x}C_{55b}{\lambda_{xz}}^{bc}(x,t)-\frac{\partial}{\partial x}{\lambda_{xz}}^b(x,t)\\&+\left(K_pE_{150b}\right)\frac{\partial^2}{\partial x^2}\varphi_s(x,t)+\left(K_pF_{150b}\right)\frac{\partial^2}{\partial x^2}\varphi_s(x,t)+(K_dE_{150b})\frac{\partial^3}{\partial x^2\partial t}\varphi_s(x,t)+(K_dF_{150b})\frac{\partial^3}{\partial x^2\partial t}\varphi_s(x,t)\\&-K_w\left(w_{0b}(x,t)\right)+K_G\left(\frac{\partial^2}{\partial x^2}w_{0b}(x,t)\right)-C_d\left(\frac{\partial}{\partial t}w_{0b}(x,t)\right)-N_0\left(\frac{\partial^2}{\partial x^2}w_{0b}(x,t)\right)=0\end{aligned}\tag{A13}$$

δw_{0c}:

$$\begin{aligned}&(I_{0c})\frac{\partial^2}{\partial t^2}w_{0c}(x,t)+(I_{1c})\frac{\partial^2}{\partial t^2}w_{1c}(x,t)+(I_{2c})\frac{\partial^2}{\partial t^2}w_{2c}(x,t)-(C_{550c})\frac{\partial}{\partial x}u_{1c}(x,t)-(C_{550c})\frac{\partial^2}{\partial x^2}w_{0t}(x,t)\\&-(C_{551c})\frac{\partial^2}{\partial x^2}w_{1c}(x,t)\text{-}2(C_{551c})\frac{\partial}{\partial x}u_{2c}(x,t)-3(C_{552c})\frac{\partial}{\partial x}u_{3c}(x,t)-(C_{552c})\frac{\partial^2}{\partial x^2}w_{2c}(x,t)-{\lambda_z}^t(x,t)\\&-{\lambda_z}^b(x,t)+\frac{\partial}{\partial x}C_{55c}{\lambda_{xz}}^{tc}(x,t)+\frac{\partial}{\partial x}C_{55c}{\lambda_{xz}}^{bc}(x,t)-N_0\left(\frac{\partial^2}{\partial x^2}w_{0c}(x,t)\right)-2N_1\left(\frac{\partial^2}{\partial x^2}w_{1c}(x,t)\right)-2N_2\left(\frac{\partial^2}{\partial x^2}w_{2c}(x,t)\right)=0\end{aligned}\tag{A14}$$

δw_{1c}:

$$\begin{aligned}&(I_{1c})\frac{\partial^2}{\partial t^2}w_{0c}(x,t)+(I_{2c})\frac{\partial^2}{\partial t^2}w_{1c}(x,t)+(I_{3c})\frac{\partial^2}{\partial t^2}w_{2c}(x,t)-(C_{552c})\frac{\partial}{\partial x}w_{1c}(x,t)-(C_{553c})\frac{\partial^2}{\partial x^2}w_{2t}(x,t)\\&+(C_{133c})\frac{\partial}{\partial x}u_{3c}(x,t)+(C_{132c})\frac{\partial}{\partial x}u_{2c}(x,t)+(C_{131c})\frac{\partial}{\partial x}u_{1c}(x,t)+(C_{130c})\frac{\partial}{\partial x}u_{0c}(x,t)\\&-(C_{551c})\frac{\partial}{\partial x}u_{1c}(x,t)\text{-}2(C_{552c})\frac{\partial}{\partial x}u_{2c}(x,t)-3(C_{553c})\frac{\partial}{\partial x}u_{3c}(x,t)-(C_{551c})\frac{\partial^2}{\partial x^2}w_{0c}(x,t)\\&+2(C_{331c})w_{2c}(x,t)+(C_{330c})w_{1c}(x,t)+\frac{h_c}{2}{\lambda_z}^t(x,t)-\frac{h_c}{2}{\lambda_z}^b(x,t)+\frac{\partial}{\partial x}h_cC_{55c}{\lambda_{xz}}^{tc}(x,t)\\&-\frac{\partial}{\partial x}h_cC_{55c}{\lambda_{xz}}^{bc}(x,t)-2N_1\left(\frac{\partial^2}{\partial x^2}w_{0c}(x,t)\right)-N_2\left(\frac{\partial^2}{\partial x^2}w_{1c}(x,t)\right)-2N_3(\frac{\partial^2}{\partial x^2}w_{2c}(x,t))=0\end{aligned}\tag{A15}$$

δw_{2c}:

$$\begin{aligned}&(I_{2c})\frac{\partial^2}{\partial t^2}w_{0c}(x,t)+(I_{3c})\frac{\partial^2}{\partial t^2}w_{1c}(x,t)+(I_{4c})\frac{\partial^2}{\partial t^2}w_{2c}(x,t)-(C_{552c})\frac{\partial}{\partial x}w_{0c}(x,t)-(C_{553c})\frac{\partial^2}{\partial x^2}w_{1t}(x,t)\\&+2(C_{134c})\frac{\partial}{\partial x}u_{3c}(x,t)+2(C_{133c})\frac{\partial}{\partial x}u_{2c}(x,t)+2(C_{132c})\frac{\partial}{\partial x}u_{1c}(x,t)+2(C_{131c})\frac{\partial}{\partial x}u_{0c}(x,t)\\&-(C_{552c})\frac{\partial}{\partial x}u_{1c}(x,t)-2(C_{553c})\frac{\partial}{\partial x}u_{2c}(x,t)-3(C_{554c})\frac{\partial}{\partial x}u_{3c}(x,t)-(C_{554c})\frac{\partial^2}{\partial x^2}w_{2c}(x,t)\\&+2(C_{331c})w_{1c}(x,t)+4(C_{332c})w_{2c}(x,t)-\frac{{h_c}^2}{4}{\lambda_z}^t(x,t)-\frac{{h_c}^2}{4}{\lambda_z}^b(x,t)+\frac{3}{4}{h_c}^2C_{55c}\frac{\partial}{\partial x}{\lambda_{xz}}^{tc}(x,t)\\&-\frac{3}{4}{h_c}^2\frac{\partial}{\partial x}C_{55c}{\lambda_{xz}}^{bc}(x,t)-2N_2\left(\frac{\partial^2}{\partial x^2}w_{0c}(x,t)\right)-2N_3\left(\frac{\partial^2}{\partial x^2}w_{1c}(x,t)\right)-N_4\left(\frac{\partial^2}{\partial x^2}w_{2c}(x,t)\right)=0\end{aligned}\tag{A16}$$

$\delta\varphi_{st}$:

$$\begin{aligned}&(E_{150t})\frac{\partial}{\partial x}u_{1t}(x,t)+(F_{150t})\frac{\partial}{\partial x}u_{1t}(x,t)+(2E_{151t})\frac{\partial}{\partial x}u_{2t}(x,t)+2(F_{151t})\frac{\partial}{\partial x}u_{2t}(x,t)+(3E_{152t})\frac{\partial}{\partial x}u_{3t}(x,t)\\&+3(F_{152t})\frac{\partial}{\partial x}u_{3t}(x,t)+(E_{150t})\frac{\partial^2}{\partial x^2}w_{0t}(x,t)+(F_{150t})\frac{\partial^2}{\partial x^2}w_{0t}(x,t)+(S_{110t})\frac{\partial^2}{\partial x^2}\varphi_s(x,t)\\&+2(S_{1100t})\frac{\partial^2}{\partial x^2}\varphi_s(x,t)+C_{110ct}\frac{\partial^2}{\partial x^2}\varphi_s(x,t)-F_{310t}\frac{\partial}{\partial x}u_{0t}(x,t)+E_{310t}\frac{\partial}{\partial x}u_{0t}(x,t)\\&-F_{311t}\frac{\partial}{\partial x}u_{1t}(x,t)+E_{311t}\frac{\partial}{\partial x}u_{1t}(x,t)-F_{312t}\frac{\partial}{\partial x}u_{2t}(x,t)+E_{312t}\frac{\partial}{\partial x}u_{2t}(x,t)-F_{313t}\frac{\partial}{\partial x}u_{3t}(x,t)\\&+E_{313t}\frac{\partial}{\partial x}u_{3t}(x,t)-\frac{\pi^2}{{h_t}^2}C_{330ct}\varphi_s(x,t)+\frac{2\pi^2}{{h_t}^2}S_{3300t}\varphi_s(x,t)-\frac{\pi^2}{{h_t}^2}s_{330t}\varphi_s(x,t)=0\end{aligned}\tag{A17}$$

$\delta{\lambda_x}^t$:

$$u_{0t}(x,t)-u_{0c}(x,t)+\frac{h_t}{2}u_{1t}(x,t)+\frac{h_c}{2}u_{1c}(x,t)+\frac{{h_t}^2}{4}u_{2t}(x,t)-\frac{{h_c}^2}{4}u_{2c}(x,t)+\frac{{h_t}^3}{8}u_{3t}(x,t)+\frac{{h_c}^3}{8}u_{3c}(x,t)=0\tag{A18}$$

$\delta\lambda_x{}^b$:

$$u_{0\mathrm{b}}(\mathrm{x},\mathrm{t}) - u_{0c}(\mathrm{x},\mathrm{t}) - \frac{h_b}{2}u_{1\mathrm{b}}(\mathrm{x},\mathrm{t}) - \frac{h_c}{2}u_{1\mathrm{c}}(\mathrm{x},\mathrm{t}) + \frac{{h_b}^2}{4}u_{2\mathrm{t}}(\mathrm{x},\mathrm{t}) - \frac{{h_c}^2}{4}u_{2\mathrm{c}}(\mathrm{x},\mathrm{t}) + \frac{{h_b}^3}{8}u_{3\mathrm{t}}(\mathrm{x},\mathrm{t}) + \frac{{h_c}^3}{8}u_{3\mathrm{c}}(\mathrm{x},\mathrm{t}) = 0 \tag{A19}$$

$\delta\lambda_z{}^t$:

$$w_{0\mathrm{t}}(\mathrm{x},\mathrm{t}) - w_{0c}(\mathrm{x},\mathrm{t}) + \frac{h_c}{2}w_{1\mathrm{c}}(\mathrm{x},\mathrm{t}) - \frac{{h_c}^2}{4}w_{2\mathrm{c}}(\mathrm{x},\mathrm{t}) = 0 \tag{A20}$$

$\delta\lambda_z{}^b$:

$$w_{0\mathrm{b}}(\mathrm{x},\mathrm{t}) - w_{0c}(\mathrm{x},\mathrm{t}) - \frac{h_c}{2}w_{1\mathrm{c}}(\mathrm{x},\mathrm{t}) - \frac{{h_c}^2}{4}w_{2\mathrm{c}}(\mathrm{x},\mathrm{t}) = 0 \tag{A21}$$

$\delta\lambda_{xz}{}^t$:

$$u_{1\mathrm{t}}(\mathrm{x},\mathrm{t}) + \frac{\partial}{\partial x}w_{0t}(\mathrm{x},\mathrm{t}) - \mathrm{h}_t u_{2\mathrm{t}}(\mathrm{x},\mathrm{t}) + \frac{3{h_t}^2}{4}u_{3\mathrm{t}}(\mathrm{x},\mathrm{t}) = 0 \tag{A22}$$

$\delta\lambda_{xz}{}^{tc}$:

$$u_{1\mathrm{b}}(\mathrm{x},\mathrm{t}) + \frac{\partial}{\partial x}w_{0b}(\mathrm{x},\mathrm{t}) - \mathrm{h}_b u_{2\mathrm{b}}(\mathrm{x},\mathrm{t}) + \frac{3{h_b}^2}{4}u_{3\mathrm{b}}(\mathrm{x},\mathrm{t}) = 0 \tag{A23}$$

$\delta\lambda_{xz}{}^{tc}$:

$$\begin{aligned} &C_{55t}\left[u_{1\mathrm{t}}(\mathrm{x},\mathrm{t}) + \frac{\partial}{\partial x}w_{0t}(\mathrm{x},\mathrm{t}) + \mathrm{h}_t u_{2\mathrm{t}}(\mathrm{x},\mathrm{t}) + \frac{3{h_t}^2}{4}u_{3\mathrm{t}}(\mathrm{x},\mathrm{t})\right] \\ &-C_{55c}\left[u_{1\mathrm{c}}(\mathrm{x},\mathrm{t}) + \frac{\partial}{\partial x}w_{0c}(\mathrm{x},\mathrm{t}) - h_c u_{2\mathrm{c}}(\mathrm{x},\mathrm{t}) + \frac{3{h_c}^2}{4}u_{3\mathrm{c}}(\mathrm{x},\mathrm{t}) - \frac{h_c}{2}w_{1\mathrm{c}}(\mathrm{x},\mathrm{t}) + \frac{{h_c}^2}{4}\frac{\partial}{\partial x}w_{2\mathrm{c}}(\mathrm{x},\mathrm{t})\right] = 0 \end{aligned} \tag{A24}$$

$\delta\lambda_{xz}{}^{bc}$:

$$\begin{aligned} &C_{55b}\left[u_{1\mathrm{b}}(\mathrm{x},\mathrm{t}) + \frac{\partial}{\partial x}w_{0b}(\mathrm{x},\mathrm{t}) - \mathrm{h}_b u_{2\mathrm{b}}(\mathrm{x},\mathrm{t}) + \frac{3{h_t}^2}{4}u_{3\mathrm{b}}(\mathrm{x},\mathrm{t})\right] \\ &-C_{55c}\left[u_{1\mathrm{c}}(\mathrm{x},\mathrm{t}) + \frac{\partial}{\partial x}w_{0c}(\mathrm{x},\mathrm{t}) - \mathrm{h}_c u_{2\mathrm{c}}(\mathrm{x},\mathrm{t}) + \frac{3{h_c}^2}{4}u_{3\mathrm{c}}(\mathrm{x},\mathrm{t})\frac{h_c}{2}w_{1\mathrm{c}}(\mathrm{x},\mathrm{t}) + \frac{{h_c}^2}{4}\frac{\partial}{\partial x}w_{2\mathrm{c}}(\mathrm{x},\mathrm{t})\right] = 0 \end{aligned} \tag{A25}$$

$\delta\varphi_{sb}$:

$$\begin{aligned} &(K_d E_{150\mathrm{b}})\frac{\partial^3}{\partial x^2\partial t}w_{0\mathrm{b}}(\mathrm{x},\mathrm{t}) + (K_d F_{150\mathrm{b}})\frac{\partial^3}{\partial x^2\partial t}w_{0\mathrm{b}}(\mathrm{x},\mathrm{t}) - (2\mathrm{K}_d E_{151\mathrm{b}})\frac{\partial^2}{\partial x\partial t}u_{2\mathrm{b}}(\mathrm{x},\mathrm{t}) + 2(K_d F_{151\mathrm{b}})\frac{\partial^2}{\partial x\partial t}u_{2\mathrm{b}}(\mathrm{x},\mathrm{t}) \\ &-(3\mathrm{K}_d E_{152\mathrm{b}})\frac{\partial^2}{\partial x\partial t}u_{3\mathrm{b}}(\mathrm{x},\mathrm{t}) + 3(K_d F_{152\mathrm{b}})\frac{\partial^2}{\partial x\partial t}u_{3\mathrm{b}}(\mathrm{x},\mathrm{t}) - (K_p E_{150\mathrm{b}})\frac{\partial^2}{\partial x^2}w_{0\mathrm{b}}(\mathrm{x},\mathrm{t}) + (K_p F_{150\mathrm{b}})\frac{\partial^2}{\partial x^2}w_{0\mathrm{b}}(\mathrm{x},\mathrm{t}) \\ &+(K_d E_{150\mathrm{b}})\frac{\partial^2}{\partial x\partial t}u_{1\mathrm{b}}(\mathrm{x},\mathrm{t}) + (K_d F_{150\mathrm{b}})\frac{\partial^2}{\partial x\partial t}u_{1\mathrm{b}}(\mathrm{x},\mathrm{t}) - \mathrm{K}_d F_{310\mathrm{b}}\frac{\partial^2}{\partial x\partial t}u_{0\mathrm{b}}(\mathrm{x},\mathrm{t}) + \mathrm{K}_d E_{310\mathrm{b}}\frac{\partial^2}{\partial x\partial t}u_{0\mathrm{b}}(\mathrm{x},\mathrm{t}) \\ &-\mathrm{K}_d F_{311\mathrm{b}}\frac{\partial^2}{\partial x\partial t}u_{1\mathrm{b}}(\mathrm{x},\mathrm{t}) + \mathrm{K}_d E_{311\mathrm{b}}\frac{\partial^2}{\partial x\partial t}u_{1\mathrm{b}}(\mathrm{x},\mathrm{t}) - \mathrm{K}_d F_{312\mathrm{b}}\frac{\partial^2}{\partial x\partial t}u_{2\mathrm{b}}(\mathrm{x},\mathrm{t}) + \mathrm{K}_d E_{312\mathrm{b}}\frac{\partial^2}{\partial x\partial t}u_{2\mathrm{b}}(\mathrm{x},\mathrm{t}) \\ &-\mathrm{K}_d F_{313\mathrm{b}}\frac{\partial^2}{\partial x\partial t}u_{3\mathrm{b}}(\mathrm{x},\mathrm{t}) + \mathrm{K}_d E_{313\mathrm{b}}\frac{\partial^2}{\partial x\partial t}u_{3\mathrm{b}}(\mathrm{x},\mathrm{t}) + (K_p E_{150\mathrm{b}})\frac{\partial}{\partial x}u_{1\mathrm{b}}(\mathrm{x},\mathrm{t}) + (K_p F_{150\mathrm{b}})\frac{\partial}{\partial x}u_{1b}(\mathrm{x},\mathrm{t}) \\ &+(2\mathrm{K}_p E_{151\mathrm{b}})\frac{\partial}{\partial x}u_{2\mathrm{b}}(\mathrm{x},\mathrm{t}) + (2\mathrm{K}_p F_{151\mathrm{b}})\frac{\partial}{\partial x}u_{2\mathrm{b}}(\mathrm{x},\mathrm{t}) + (3\mathrm{K}_p F_{152\mathrm{b}})\frac{\partial}{\partial x}u_{3\mathrm{b}}(\mathrm{x},\mathrm{t}) + (3\mathrm{K}_p E_{152\mathrm{b}})\frac{\partial}{\partial x}u_{3\mathrm{b}}(\mathrm{x},\mathrm{t}) \\ &-(K_p F_{310\mathrm{b}})\frac{\partial}{\partial x}u_{0\mathrm{b}}(\mathrm{x},\mathrm{t}) + (K_p E_{310\mathrm{b}})\frac{\partial}{\partial x}u_{0\mathrm{b}}(\mathrm{x},\mathrm{t}) - (K_p F_{311\mathrm{b}})\frac{\partial}{\partial x}u_{1\mathrm{b}}(\mathrm{x},\mathrm{t}) + (K_p E_{311\mathrm{b}})\frac{\partial}{\partial x}u_{1\mathrm{b}}(\mathrm{x},\mathrm{t}) \\ &-(K_p F_{312\mathrm{b}})\frac{\partial}{\partial x}u_{2\mathrm{b}}(\mathrm{x},\mathrm{t}) + (K_p E_{312\mathrm{b}})\frac{\partial}{\partial x}u_{2\mathrm{b}}(\mathrm{x},\mathrm{t}) - (K_p F_{313\mathrm{b}})\frac{\partial}{\partial x}u_{3\mathrm{b}}(\mathrm{x},\mathrm{t}) + (K_p E_{313\mathrm{b}})\frac{\partial}{\partial x}u_{3\mathrm{b}}(\mathrm{x},\mathrm{t}) \\ &+\mathrm{K}_p{}^2 S_{110\mathrm{b}}\frac{\partial^2}{\partial x^2}\varphi_s(\mathrm{x},\mathrm{t}) + 2\mathrm{K}_p{}^2 S_{1100\mathrm{b}}\frac{\partial^2}{\partial x^2}\varphi_s(\mathrm{x},\mathrm{t}) + \mathrm{K}_p{}^2 C_{110\mathrm{b}}\frac{\partial^2}{\partial x^2}\varphi_s(\mathrm{x},\mathrm{t}) + 2\mathrm{K}_p K_d S_{110\mathrm{b}}\frac{\partial^3}{\partial x^2\partial t}\varphi_s(\mathrm{x},\mathrm{t}) \\ &+4\mathrm{K}_p K_d S_{1100\mathrm{b}}\frac{\partial^3}{\partial x^2\partial t}\varphi_s(\mathrm{x},\mathrm{t}) + 2\mathrm{K}_p K_d C_{110\mathrm{b}}\frac{\partial^3}{\partial x^2\partial t}\varphi_s(\mathrm{x},\mathrm{t}) + \mathrm{K}_p K_d S_{110\mathrm{b}}\frac{\partial^4}{\partial x^2\partial t^2}\varphi_s(\mathrm{x},\mathrm{t}) + 2\mathrm{K}_p K_d S_{1100\mathrm{b}}\frac{\partial^4}{\partial x^2\partial t^2}\varphi_s(\mathrm{x},\mathrm{t}) \\ &+\mathrm{K}_p K_d C_{110\mathrm{b}}\frac{\partial^4}{\partial x^2\partial t^2}\varphi_s(\mathrm{x},\mathrm{t}) - \frac{\pi^2}{{h_a}^2}K_p K_d C_{330\mathrm{b}}\frac{\partial^2}{\partial t^2}\varphi_s(\mathrm{x},\mathrm{t}) + \frac{2\pi^2}{{h_a}^2}K_p K_d S_{3300\mathrm{b}}\frac{\partial^2}{\partial t^2}\varphi_s(\mathrm{x},\mathrm{t}) - \frac{\pi^2}{{h_a}^2}K_p K_d S_{330\mathrm{b}}\frac{\partial^2}{\partial t^2}\varphi_s(\mathrm{x},\mathrm{t}) \\ &-\frac{\pi^2}{{h_a}^2}K_p{}^2 C_{330\mathrm{b}}\frac{\partial^2}{\partial t^2}\varphi_s(\mathrm{x},\mathrm{t}) + \frac{2\pi^2}{{h_a}^2}K_p{}^2 S_{3300\mathrm{b}}\frac{\partial^2}{\partial t^2}\varphi_s(\mathrm{x},\mathrm{t}) - \frac{2\pi^2}{{h_a}^2}K_p{}^2 S_{330\mathrm{b}}\frac{\partial^2}{\partial t^2}\varphi_s(\mathrm{x},\mathrm{t}) - \frac{2\pi^2}{{h_a}^2}K_p K_d S_{330\mathrm{b}}\frac{\partial}{\partial t}\varphi_s(\mathrm{x},\mathrm{t}) \\ &-\frac{2\pi^2}{{h_a}^2}K_p K_d C_{330\mathrm{b}}\frac{\partial}{\partial t}\varphi_s(\mathrm{x},\mathrm{t}) + \frac{4\pi^2}{{h_a}^2}K_p K_d S_{3300\mathrm{b}}\frac{\partial}{\partial t}\varphi_s(\mathrm{x},\mathrm{t}) = 0 \end{aligned} \tag{A26}$$

Appendix B

$$I_{0i}, I_{1i}, I_{2i}, I_{3i}, I_{4i}, I_{5i}, I_{6i} = \int_{-x}^{x} \rho_i(z)(1, z, z^2, z^3, z^4, z^5, z^6)dz \tag{B1}$$

$$C_{110i}, C_{111i}, C_{112i}, C_{113i}, C_{114i}, C_{115i}, C_{116i} = \int_{-x}^{x} C_{11i}(z)(z^0, z, z^2, z^3, z^4, z^5, z^6)dz \tag{B2}$$

$$C_{550i}, C_{551i}, C_{552i}, C_{553i}, C_{554i}, C_{555i} = \int_{-x}^{x} C_{55i}(z)(z^0, z, z^2, z^3, z^4, z^5)dz \tag{B3}$$

$$C_{130c}, C_{131c}, C_{132c}, C_{133c}, C_{134c} = \int_{-\frac{h_c}{2}}^{\frac{h_c}{2}} C_{13c}(z)(z^0, z, z^2, z^3, z^4)dz \tag{B4}$$

$$C_{330c}, C_{331c}, C_{332c}, C_{333c}, C_{334c} = \int_{-\frac{h_c}{2}}^{\frac{h_c}{2}} C_{33c}(z)(z^0, z, z^2, z^3, z^4)dz \tag{B5}$$

$$N_{0i} = \int_{-x}^{x} C_{11}\alpha(t)\Delta T dz \tag{B6}$$

$$N_{0c}, N_{1c}, N_{1c}, N_{1c}, N_{1c} = \int_{-\frac{h_c}{2}}^{\frac{h_c}{2}} E_c\alpha(t)\Delta T(z, z^2, z^3, z^4)dz \tag{B7}$$

$$F_{310j}, F_{311j}, F_{312j}, F_{313j}, F_{314j} = \int_{-y}^{y} e_{31} cos\left(\frac{\pi z}{h_j}\right) cos\left(\frac{\pi h_c}{2h_j}\right)\frac{\pi}{h_j}(z^0, z, z^2, z^3, z^4)dz \tag{B8}$$

$$F_{150j}, F_{151j}, F_{152j} = \int_{-y}^{y} e_{15} cos\left(\frac{\pi z}{h_j}\right) cos\left(\frac{\pi h_c}{2h_j}\right)\frac{\pi}{h_j}(z^0, z, z^2)dz \tag{B9}$$

$$E_{310j}, E_{311j}, E_{312j}, E_{313j}, E_{314j} = \int_{-y}^{y} e_{31} sin\left(\frac{\pi z}{h_j}\right) sin\left(\frac{\pi h_c}{2h_j}\right)\frac{\pi}{h_j}(z^0, z, z^2, z^3, z^4)dz \tag{B10}$$

$$E_{150j}, E_{151j}, E_{152j} = \int_{-y}^{y} e_{15} sin\left(\frac{\pi z}{h_j}\right) sin\left(\frac{\pi h_c}{2h_j}\right)\frac{\pi}{h_j}(z^0, z, z^2)dz \tag{B11}$$

$$S_{110j} = \int_{-y}^{y} k_{11}\left(sin\left(\frac{\pi z}{h_j}\right)\right)^2\left(cos\left(\frac{\pi h_c}{2h_j}\right)\right)^2 dz \tag{B12}$$

$$C_{110cj} = \int_{-y}^{y} k_{11}\left(cos\left(\frac{\pi z}{h_j}\right)\right)^2\left(sin\left(\frac{\pi h_c}{2h_j}\right)\right)^2 dz \tag{B13}$$

$$S_{330j} = \int_{-y}^{y} k_{33}\left(sin\left(\frac{\pi z}{h_j}\right)\right)^2\left(cos\left(\frac{\pi h_c}{2h_j}\right)\right)^2 dz \tag{B14}$$

$$C_{330cj} = \int_{-y}^{y} k_{33}\left(cos\left(\frac{\pi z}{h_j}\right)\right)^2\left(sin\left(\frac{\pi h_c}{2h_j}\right)\right)^2 dz \tag{B15}$$

$$S_{3300j} = \int_{-y}^{y} k_{33}\left(sin\left(\frac{\pi z}{h_j}\right)\right)\left(cos\left(\frac{\pi h_c}{2h_j}\right)\right)\left(cos\left(\frac{\pi z}{h_j}\right)\right)\left(sin\left(\frac{\pi h_c}{2h_j}\right)\right)dz \tag{B16}$$

$$N_y = \int_{-\frac{h_b}{2}}^{\frac{h_b}{2}} e_{31}V_0 dz \tag{B17}$$

$$y = \left(\frac{h_t}{2}, \frac{h_b}{2}\right), \qquad j = t, b$$
$$x = \left(\frac{h_t}{2}, \frac{h_c}{2}, \frac{h_b}{2}\right), \qquad i = t, b, c$$